Title: An integrated investigation of the effects of ocean acidification on adult abalone (*Haliotis tuberculata*)

Authors: Solène Avignon[1], Stéphanie Auzoux-Bordenave[1,2], Sophie Martin[2,3], Philippe Dubois[4], Aïcha Badou[5], Manon Coheleach[6], Nicolas Richard[1], Sarah Di Giglio[4], Loïc Malet[7], Arianna Servili[8], Fanny Gaillard[3], Sylvain Huchette[9] and Sabine Roussel[6]

[1]UMR "Biologie des Organismes et Ecosystèmes Aquatiques" (BOREA), MNHN/CNRS/SU/IRD, Muséum national d'Histoire naturelle, Station marine de Concarneau, 29900 Concarneau, France

[2]Sorbonne Université, 4, place Jussieu, 75005 Paris, France

[3]UMR 7144 "Adaptation et Diversité en Milieu Marin" (AD2M), CNRS/SU, Station Biologique de Roscoff, 29680 Roscoff Cedex, France

[4]Laboratoire de Biologie Marine, Université Libre de Bruxelles, CP160/15, 1050, Brussels, Belgium

[5]Direction Générale Déléguée à la Recherche, l'Expertise, la Valorisation et l'Enseignement (DGD REVE), Muséum national d'Histoire naturelle, Station marine de Concarneau, 29900 Concarneau, France

[6]Université de Brest, CNRS, IRD, Ifremer, LEMAR, F-29280 Plouzané, France

[7]Service 4Mat, Université Libre de Bruxelles, CP 194/3, 1050 Brussels, Belgium

[8]IFREMER, Université de Brest, CNRS, IRD, LEMAR, F-29280 Plouzané, France

[9]Ecloserie France Haliotis, Kerazan, 29880 Plouguerneau, France

Corresponding author: Stéphanie Auzoux-Bordenave, Tel: +33 2 98 50 42 88, Mail: stephanie.auzoux-bordenave@mnhn.fr

Abstract

Ocean acidification (OA) and its subsequent changes in seawater carbonate chemistry are threatening the survival of calcifying organisms. Due to their use of calcium carbonate to build their shells, marine molluscs being particularly vulnerable. This study investigated the effect of CO_2-induced OA on adult European abalone (*Haliotis tuberculata*) using a multi-parameter approach. Biological (survival, growth), physiological (pH_T of haemolymph, phagocytosis, metabolism, gene expression) and structural responses (shell strength, nanoindentation measurements, SEM imaging of microstructure) were evaluated throughout a 5-month exposure to ambient (8.0) and low (7.7) pH conditions. During the first two months, the haemolymph pH was reduced, indicating that abalone do not compensate for the pH decrease of their internal fluid. Overall metabolism and immune status were not affected, suggesting that abalone maintain their vital functions when facing OA. However, after four months of exposure, adverse effects on shell growth, calcification, microstructure and resistance were highlighted, whereas the haemolymph pH was compensated. Significant reduction in shell mechanical properties were revealed at pH 7.7, suggesting that OA altered the biomineral architecture leading to a more fragile shell. It is concluded that under lower pH, abalone metabolism is maintained at a cost to growth and shell integrity. This may impact both abalone ecology and aquaculture.

Keywords: abalone, calcification, gene expression, growth, mechanical properties, ocean acidification, physiology, shell microstructure

Introduction

Over the past 200 years, about one-third of anthropogenic CO_2 emissions have been absorbed by the oceans, resulting in a disruption of carbonate chemistry (Caldeira and Wickett, 2003; Sabine *et al.*, 2004). These changes in the carbonate balance are responsible for a decrease of seawater pH and the lowering of calcium carbonate ($CaCO_3$) saturation state, a process known as ocean acidification (OA) (Caldeira and Wickett, 2003; Hoegh-Guldberg *et al.*, 2007; Gattuso *et al.*, 2015). Predictive scenarios suggest a decrease in seawater pH of 0.1 to 0.4 unit by the end of the 21st century (Orr *et al.*, 2005; IPCC, 2014; Gattuso *et al.*, 2015). OA may affect organisms producing calcium carbonate shells, tests or skeletons, such as molluscs, corals and echinoderms, to different extents (Hendriks *et al.,* 2010; Hofmann *et al.*, 2010; Wittmann and Pörtner, 2013; Cyronak *et al.,* 2016). Due to their physiological characteristics and their use of $CaCO_3$ to build their shell, marine molluscs are among the most vulnerable species with regard to OA (Fabry, 2008; Gazeau *et al.*, 2013; Kroeker *et al.*, 2013; Parker *et al.*, 2013). Since proton export from the calcifying space is more energy demanding under OA, metabolic energy demand forcibly rises (Beniash *et al.*, 2010; Parker *et al.*, 2012). Indeed, many species show reduced calcification rates when exposed to acidified seawater (Michaelidis *et al.*, 2005; Gazeau *et al.*, 2007). Furthermore, shell structural and mechanical properties may be affected (Fitzer *et al.*, 2015).

Abalone are ecologically and commercially important molluscs providing essential ecosystem services and food delicacy for humans (Cook, 2016). The European species, *Haliotis tuberculata*, is traditionally eaten in Brittany, the Channel Islands and in some parts of the Mediterranean (Huchette and Clavier, 2004). Whereas production from abalone fisheries worldwide has declined from 20 000 tons in the 1970s to around 6 500 tons in recent times due to overfishing and environmental disruptions (Vilchis *et al.*, 2005; Rogers-Bennett, 2007; Travers *et al.*, 2009; Cook, 2016), abalone aquaculture production has significantly increased

78 over the past few years from a negligible quantity in the 1970s to 130 000 tons in 2015 (Cook,
79 2016). Understanding the effects of environmental stress on abalone biology is an important
80 issue for the management of natural populations as well as for the optimization of fisheries
81 and aquaculture practices (Morash and Alter, 2015).

82 *H. tuberculata* is a suitable model for studying the calcification process under OA, since its
83 shell is mainly composed of aragonite (Auzoux-Bordenave *et al.*, 2010), a calcium-carbonate
84 polymorph, which is more sensitive to dissolution than calcite (Morse *et al.*, 2007). Captive
85 rearing of abalone is possible for the entire life cycle, making it possible to study the effects
86 of OA under controlled conditions on different development stages (Wessel *et al.*, 2018).
87 Recent study on *H. tuberculata* has shown that larval viability and development were
88 negatively affected at lower pH (7.7 and 7.6) while larval shell showed a reduction in
89 mineralization (Wessel *et al.*, 2018). Adverse effects of OA were also shown in six-month old
90 juvenile, with significant decreases in growth and changes in shell microstructure (Auzoux-
91 Bordenave *et al.*, 2019). As suggested by previous studies, the exposure of adult molluscs to
92 OA might also influence shell growth, calcification and offspring survival (Parker *et al.*,
93 2013). For example, the intertidal common limpet *Patella vulgata* exposed for a few days to
94 lower pH (7.6) was able to maintain its extracellular acid-base balance, metabolism and
95 feeding rate, but damage was sustained to the radula of adults which could compromise
96 feeding and population survival (Marchant *et al.*, 2010). In adult oyster *Crassostrea virginica*,
97 physiology and rates of shell deposition appeared to be negatively affected by OA, with an
98 increase in carbonic anhydrase expression in tissues of animals exposed to reduced pH water
99 (Beniash *et al.*, 2010). So far, no studies have been conducted on the adult stage of European
100 abalone *H. tuberculata*.

101 The goal of the present study was to investigate the effects of a five-month exposure to CO_2-
102 induced OA on adult abalone using a multi-parameter approach. Four-year abalone *H.*

tuberculata were exposed during reproductive conditioning to ambient seawater pH (8.0) and to a lower pH value (7.7) corresponding to the projected decrease of -0.3 pH units under RCP 8.5 climate change scenario (IPCC, 2014; Gattuso *et al.*, 2015). Several biological parameters involved in growth, physiology and metabolism were measured on individuals exposed to either current or near-future pH conditions. Shell microstructure and mechanical properties were also analysed to assess whether reduced pH has an influence on shell integrity.

Material and methods

Abalone collection and acclimation

Adult *H. tuberculata* (n = 260, 48.5 ± 4.2 mm shell length, 16.2 ± 4.4 g shell weight), from a spawning performed during summer 2013, were selected at random from an offshore sea-cage structure containing 600 individuals per cage, at the France Haliotis abalone farm in January 2017 (48°36'50N, 4°36'3W; Plouguerneau, Brittany, France). Fresh algae collected on the shore were provided *ad libitum* to each sea-cage once a month. The algae were composed of mixture of *Palmaria palmata*, *Laminaria digitata* and *Saccharina latissima*, depending on the season (S. Huchette, pers. comm.). Abalone were brought to the France Haliotis land-based facilities ensuring minimum stress during transport and minimum handling. After measuring size and weight, each abalone was randomly distributed in ten 45 L aquaria (l × w × h, 50 × 30 × 35 cm) equipped with baked clay hiding places (n = 26 abalone per aquarium). An aeration system was placed in each aquarium. Animals were conditioned for three weeks in the laboratory under ambient pCO_2/pH conditions, in aquaria supplied with a minimum of 15 L/h of 3 µm filtered seawater at ambient temperature. The seawater was pumped from close to the farm. During the experimentation, abalone were fed once a week *ad libitum* with the

126 macroalgae *P. palmata*. The aquaria were cleaned twice a week using a siphoning hose and
127 water filters were changed every day.

128 ***Experimental set-up***

129 Each experimental aquarium was randomly assigned to one of two pH treatments (Figure 1): a
130 control condition corresponding to the local seawater pH (8.0, pCO_2 around 460 µatm) and a
131 lower pH value (7.7, pCO_2 around 1000 µatm) corresponding to the projected decrease of -0.3
132 pH units under climate change scenario RCP 8.5 (IPCC, 2014; Gattuso *et al.*, 2015). Five
133 replicate aquaria were used per pH condition. Photoperiod was adjusted following the
134 seasonal cycle with a dimmer (Gold Star, Besser Elektronik, Italy). The experiment was
135 carried out for five months between February and July 2017. At the beginning of the
136 experiment, pH was gradually decreased over six days by 0.05 pH units / day until pH 7.7 was
137 reached.

138 ***pH and carbonate system monitoring***

139 Inside a storage tank (9000 L), seawater was temperature-controlled with a heat pump and
140 used to continuously fill the ten header tanks. Each header tank supplied one experimental
141 tank at a rate of 15 L/h. In the five CO_2-enriched header tanks, pCO_2 was adjusted by
142 bubbling CO_2 (Air Liquide, France) through electro-valves controlled by a pH-stat system
143 (IKS Aquastar, Germany). pH values of the pH-stat system were adjusted from measurements
144 of the electromotive force using a pH meter (Metrohm 826 pH mobile, Metrohm,
145 Switzerland) with a glass electrode (Primatrode). The electromotive force was converted to
146 pH units on the total scale (pH_T) after calibration with Tris/HCl and 2-aminopyridine/HCl
147 buffers (Dickson, 2010).

148 Seawater parameters were recorded every three days throughout the five-month experiment.
149 Temperature was regulated at 2 °C above the monthly average temperature observed in local

environment (10.5 °C in January to 16.5 °C in June) in order to stimulate gonad development. pH_T was measured every three days in each experimental aquaria using a pH meter as described above. Temperature and salinity were measured daily with a conductimeter (WTW 3110, Germany). Total alkalinity (A_T) of seawater was measured monthly on 100-mL samples taken from incoming water and from each experimental tank. Seawater samples were filtered through 0.7-µm Whatman GF/F membranes, immediately poisoned with mercuric chloride and stored in a cool dark place pending analyses. A_T was determined potentiometrically using an automatic titrator (Titroline alpha, Schott SI Analytics, Germany) calibrated with the National Bureau of Standards scale. A_T was calculated using a Gran function applied to pH values ranging from 3.5 to 3.0 as described by Dickson *et al.* (2007) and corrected by comparison with standard reference material provided by A. G. Dickson (CRM Batch 111). Temperature, salinity, pH_T and A_T were used to calculate the carbonate system parameters: pCO_2, dissolved inorganic carbon (DIC), HCO_3^-, CO_3^{2-} concentrations, and saturation state of aragonite ($\Omega_{aragonite}$) and calcite ($\Omega_{calcite}$). Calculations were performed using CO_2SYS software (Pierrot *et al.*, 2006) set with constants of Mehrbach *et al.* (1973) refitted by Dickson and Millero (1987).

Abalone sampling

The effects of OA were examined at different sampling times. Firstly, the short-term exposure response was analysed after one week (W1, 6 days) of pH exposure. Afterwards, samplings were done regularly every month: at two months (M2, 60 days), three months (M3, 90 days), four months (M4, 125 days) and five months (M5, 157 days).

At each sampling time, abalone were randomly collected for biometric measurements. Physiological measurements were performed on haemolymph sampled for some individuals (see below), while metabolic parameters were measured on live animals. Mantle tissue was dissected and rapidly frozen in liquid nitrogen for gene expression analyses. The shells were

rinsed with distilled water, dried and stored at room temperature until analysis. Abalone were only used once in the experiment and were not returned to the aquaria after measurement. Some individuals were used for two types of measures (e.g., physiological and biometric measures).

Survival

Abalone survival was assessed every day along the experiment and any dead individuals were removed from the tanks immediately. Survival (%) was calculated as the proportion of living individuals after the five-month treatment vs total number of abalone per aquarium at the beginning of the experiment, minus the individuals sacrificed for analysis.

Biometric measurements

Biometric measurements were performed at W1, M2, M3, M4 and M5 of exposure. At each sampling time, length (mm) was measured using a manual calliper to the nearest 0.5 mm to obtain the growth in length in mm/day on two to five abalone per aquarium (n = 13 to 39 abalone per pH treatment). Except at M5, individuals were weighed using an analytical balance to the nearest 0.01 mg to obtain specific growth rate using natural log mass values (% gain/day). Haemolymph was sampled in less than 1 minute from the pedal sinus, using a refrigerated 2-mL syringe and 25 G x ½ needles. It was transferred to a vial on ice and processed immediately after collection to avoid haemocyte aggregation. After a section of the head, tissues and organs were dissected. The weight of the foot muscle, gonad, shell, and haemolymph were recorded to the nearest 0.01 mg.

Physiological measurements

The pH_T of the haemolymph was measured immediately on two abalone per aquarium (n = 10 per pH treatment), at W1, M2 and M4. The electromotive force of the haemolymph was measured with a glass electrode put into the vial. Temperature was also measured to obtain

199 pH_T according to the procedure described above for seawater pH_T determination.
200 Phagocytosis efficiency was measured according to a protocol adapted from Travers *et al.*
201 (2008), using two replicates of 25 µL haemolymph. Briefly, 25 µL of haemolymph was
202 deposited into a 24-well plate containing 100 µL of sterile seawater. Haemocytes were
203 allowed to adhere for 15 min at 18 °C. Fluorescent beads (gluoresbrite YG Microspheres 2.00
204 mm, Plysciences, 1:100 in distilled water) were added. After 2 h at 18 °C, supernatants were
205 removed and 100 µL of trypsin (2.5 $mg.mL^{-1}$ in AASH) was added to detach the adherent
206 cells. Plates were shaken for 10 min. Then, 100 µL of 6 % formalin was used to stop the
207 reaction. Analyses were performed on a FACS-Calibur flow cytometer (Becton Dickinson,
208 France) equipped with a 488-nm laser. Data were analysed using the WinMDI program.
209 Phagocytosis efficiency was defined as the percentage of haemocytes that had engulfed three
210 or more beads.

211 ***Gene expression analysis***

212 The expression profile of selected genes were analysed in the mantles of two to four
213 individual abalone per aquarium (n = 17 for pH 8.0 and n = 14 for pH 7.7) after four months
214 of pH treatment (M4). Genes were chosen with respect to their putative functions in shell
215 growth and calcification responses and their abundance in the mantle transcriptomes (Shen *et*
216 *al.*, 1997; Le Roy *et al.*, 2012). One gene involved in shell biomineralization, Lustrin A, two
217 Carbonic Anhydrases involved in bicarbonate ions formation (CA 1 and CA 2), and genes for
218 two stress proteins (heat shock proteins), HSP71 and HSP84, were targeted by using specific
219 primers (Table 1). 18S and EF1 were used as reference genes.

220

221

222 **Table 1.** Specific primers used for gene expression analysis in *Haliotis tuberculata*: Genbank
223 accession number, primer sequences and reference.

Gene	Accession number	Sequence 5'-3'	Reference
Lustrin A	HM852427.2	F-ATCTGTCCGGCAGTTCCTAC R-CTGGGGCACTGTAAGTTGGT	Gaume *et al.* (2014)
Carbonic anhydrase 1	HQ845770.1	F-ATGGCAGCTGATAAAGCAAC R-AGGGAAATGAGTGTGCATGT	Designed for the study
Carbonic anhydrase 2	HQ845771.1	F-CGCCGACTTTATCTGAGAGC R-GTCTCCCACGAAGTGGTTGT	Le Roy *et al.* (2012)
18S	AF120511.1	F-GGTTCCAGGGGAAGTATGGT R-AGGTGAGTTTTCCCGTGTTG	Gaume *et al.* (2014)
EF1	FN566842.1	F-ATTGGCCACGTAGATTCTGG R-GCTCAGCCTTCAGTTTGTCC	Gaume *et al.* (2014)
HSP 71	AM283516.1	F-CGGTGAGCGCAATGTTC R-CCAAGTGGGTGTCTCCA	Farcy *et al.* (2007)
HSP 84	AM283515.1	F-CCAGGAAGAATATGCCGAGT R-CACGGAACTCCAACTGACC	Farcy *et al.* (2007)

224

225 Frozen mantle samples were pulverized under liquid nitrogen using a Retsch MM400 mixer
226 mill. Total RNA was extracted from the resulting powder using Extract-all reagent (Eurobio,
227 Courtaboeuf, Essonne, France) followed by chloroform phase separation and isopropanol
228 precipitation. The co-extracted DNA was then digested with an RTS DNase Kit (MoBio). The
229 quantity, purity and quality of RNA were assessed using a ND-1000 NanoDrop®
230 spectrophotometer (Thermo Scientific Inc., Waltham, MA, USA) and by electrophoresis
231 using an Agilent Bioanalyser 2100 (Agilent Technologies Inc., Santa Clara, CA, USA).
232 cDNA synthesis was performed using an iScript™ cDNA Synthesis kit (Bio-Rad Laboratories

Inc., Hercules, CA, USA). Reverse transcription-quantitative PCR (RT-qPCR) was conducted in a C1000 Touch Thermal Cycler (Bio-Rad Laboratories Inc., Hercules, CA, USA) using specific primers (see Table 1) and SsoAdvanced Universal SYBR Green Supermix (Bio-Rad Laboratories Inc., Hercules, CA, USA) as described by Cadiz *et al.* (2017). Gene expression was quantified using the iCycler MyiQ™ Single Color Real-Time PCR Detection System (Bio-Rad Laboratories Inc.). The relative quantity of messenger was normalized with the ΔCt method using the same CFX Manager software (Bio-Rad Laboratories Inc.).

Metabolic rates

Calcification, respiration and excretion rates were determined using two to three individual abalone per aquarium at W1, M2 and M3 (n = 9 to 15 abalone per pH treatment). Individuals were incubated individually in a 598-mL acrylic chamber (Engineering & Design Plastics Ltd, Cambridge, UK) filled with seawater from their respective aquaria. Incubations lasted one hour. Blank incubations were also carried out with only seawater from the aquarium to adjust respiration and excretion rates.

Oxygen concentrations were measured at the beginning and the end of the incubation period with a non-invasive fiber-optics system (FIBOX 3, PreSens, Regensburg, Germany). Reactive oxygen spots attached to the inner wall of the chambers were calibrated with 0% and 100% oxygen buffers. Seawater was sampled for ammonium (NH_4^+) concentration with 100 mL syringes at the beginning of the incubation, directly in the aquaria just after the chambers were closed, and at the end of the incubation, in the incubation chamber itself. Samples were fixed with reagent solutions and stored in the dark. NH_4^+ concentrations were determined according to the Solorzano method (Solorzano, 1969) based on spectrophotometry at a wavelength of 630 nm (spectrophotometer UV-1201V, Shimadzu Corp, Kyoto, Japan). A_T (in µEq/L) values were obtained in the same way as described above in the section *pH and carbonate system monitoring*. Respiration (in µmol O_2/g WW/h; Eq. 1) and excretion (in

µmol NH_4^+/g WW/h; Eq. 2) rates were directly calculated from oxygen and ammonium concentrations, respectively. Net calcification (in µmol $CaCO_3$/g WW/h; Eq. 3) rate was estimated using the alkalinity anomaly technique (Smith and Key, 1975) based on decrease in A_T by two equivalents for each mole of $CaCO_3$ precipitated (Wolf-Gladrow *et al.*, 2007). As ammonium production increases alkalinity in a mole-per-mole ratio (Wolf-Gladrow *et al.*, 2007), the alkalinity variation was corrected by the ammonium flux to calculate $CaCO_3$ fluxes.

$$R = \frac{\Delta O_2 \times V}{\Delta t \times WW} \quad (1)$$

$$E = \frac{\Delta NH_4^+ \text{ x V}}{\Delta t \times WW} \quad (2)$$

$$G = \frac{-(\Delta A_T - \Delta NH_4) \text{ x } V}{2x\Delta txWW} \quad (3)$$

where ΔO_2 (in µmol O_2/L), ΔNH_4^+ (in µmol NH_4^+/L) and ΔA_T (in µEq/L) are the differences between initial and final O_2 concentrations, NH_4^+ concentrations and total alkalinity, respectively; V (in L) is the volume of the chamber minus *H. tuberculata* volume; Δt (in h) is the incubation time and WW (in g) is the soft tissue wet weight of the incubated *H. tuberculata*.

Shell analysis

Two to nine shells per aquarium (n = 10 to 39 abalone per pH treatment) were examined at M2, M3, M4 and M5. The thickness (mm) of the shell newly formed during the experiment was determined as the average of three measurements closest to the edge of the shell, along the growth axis (Supplementary Figure S1a) to the nearest 0.001 mm using a Mitutoyo® digital calliper. Abalone shells were imaged with the NIS elements software (Nikon, Japan) under a binocular microscope (Leica, Germany). For the evaluation of periostracum

morphology, the shell surface was imaged and analysed for differences in grey scale. Image-J software was used to calculate an average grey value from zero (black) to 255 (white). The average of grey levels was calculated from a 4 mm² area closest to the shell edge, along the growth axis (Supplementary Figure S1a).

To analyse shell surface microstructure, four abalone shells per pH treatment were randomly chosen for further investigation of the inner and outer surfaces by scanning electron microscopy, SEM (Supplementary Figure S1b). The shell was cut in order to obtain a shell fragment formed during the experiment. Samples were gold-coated (Cressington 108, Auto Sputter coater) and observed at 5–15 kV with a SEM (SEM FEI Sigma 300, MNHN, Concarneau, France).

To determine the influence of seawater acidification on shell microstructure and thickness, cross-sections were obtained using a razor blade along the longitudinal growth axis of the shell (Supplementary Figure S1c). Samples were embedded in epoxy resin, gold-coated and observed as described above. Three transects were determined on SEM images of the cross-sections: in the old part, intermediate part and newly formed shell area. Within each transect, images were generated from the outer periostracum to the inner nacreous layer, passing through the spherulitic layer.

At higher magnification, the aragonite tablet thickness (average of 25 measurement points) was determined from both old and recent nacre on SEM images with Image-J (n = 3 shells per pH treatment). The thickness of the periostracum, the spherulitic and nacreous layers were determined from the cross-section images using Image-J software (n = 5 abalone shells per treatment, 20 measurement points per layer).

303 ***Biomechanical tests***

304 Shell strength (resistance) was measured individually (n = 10 shells per pH treatment) at M4
305 using a simple compression method. The comparison of shell fracture force was performed on
306 shells with a similar size and shape. Abalone shells were placed always in a same way on a
307 homemade steel block with their opening downwards (i.e., in the natural position they would
308 have on a rocky substrate) and the mechanical test was carried out using a second homemade
309 steel block (7 x 5 x 2 cm) fixed on the load frame of a force stand (Instron 5543) through a
310 threaded shaft. Care was taken that the two blocks were strictly parallel. The second block
311 was lowered onto the shell at a speed of 0.3 mm/min (simple compression test) until fracture.
312 Displacement (mm) and compression force (N) were recorded continuously at a frequency of
313 10 Hz.

314 Nanoindentation measurements were performed to characterize the properties of the material,
315 i.e., the shell nanohardness and Young's modulus of elasticity. The other fragment obtained
316 from the earlier cross-section (for SEM) was polished using sandpapers of decreasing grain
317 size (from 52 to 5 µm) to obtain a homogeneous surface (n = 4 shells per pH treatment).
318 Nanoindentation measurements were performed using a Triboindenter (Hysitron, USA) with a
319 Berkovich tip and a charge of 1500 µN. Nanohardness (GPa) and Young's modulus of
320 elasticity (GPa) were calculated automatically from the unloading curve of the indentation
321 test. For each individual abalone, three profiles spaced by 5 to 8 mm were made in the newly
322 formed, intermediate and older zones. Each profile consisted of three continuous transects
323 through the two layers (external layer and nacre) spaced by 5 µm apart. Each transect
324 consisted of 61 indents (26 to 31 indents per layer). Because values recorded in the three
325 transects of each zone did not differ significantly, the results from the three transects were
326 pooled.

327

Statistical analysis

All statistical analyses were performed with R software (R Core Team, 2015). Differences between the two pH treatments, except for the biomechanical tests, were tested using linear mixed models with the lmerTest package (Kuznetsova *et al.*, 2017) based on the methods described by Winter (2013). This model used the pH as a fixed factor and aquarium as a random factor nested within the factor pH. Since biometric measurements were performed on abalone that had already been used for metabolism and physiological assessments (at W1, M2 and M4), a test effect was included in the mixed model for those variables. Statistical analysis was performed on the data separately for each time point. For shell, haemolymph, muscle and gonad weights, total weight was integrated as a covariate in the mixed model. A Student's t-test was used to compare the mortality and thickness of nacreous platelets between the two pH treatments. To be sure to only evaluate the effect of OA on shell resistance, the relationship between the shell fracture force and biometric parameters (shell length, weight, area and thickness) was tested using a linear regression.

The normality of the residuals and homogeneity of the variance were verified (Shapiro–Wilk and Bartlett tests). When assumptions of homogeneity of variance and normal distribution of residuals were not confirmed, the data were log or inverse transformed before analysis. If these assumptions were not validated, a Welch test was performed using the aquarium value as individual in the statistical test. Differences were considered significant at $p < 0.05$. Data are presented as means of squares ± standard error unless otherwise indicated. All results in graphs are presented as boxplots showing the median, the 2nd and 3rd quartiles (boxes), the 95% confidence interval (whiskers) and outside of the 95 percentile range values (o).

Mechanical data were analysed using the cumulative probability function:

$$P_{fi} = 1 - exp\left(-\left(\frac{\sigma_i}{\sigma_0}\right)^m\right)$$

which is also known as the Weibull three-parameter strength distribution. P_f is the probability of failure that increases with the stress variable, σ. The characteristic stress σ_0 is an experimentally obtained parameter that corresponds to a proportion of fractured samples of (1 - 1/e) = 63% (cumulative failure probability). In this study, we replaced the stress variable by nanohardness (H_0) and Young's modulus of elasticity (E_0) and used the linearized curve of Weibull statistical analysis to calculate the 95% confidence intervals of E_0 and H_0 (corresponding to the 63 percentiles for Young's modulus of elasticity and nanohardness, respectively) with the modified least square regression of Bütikofer *et al.*(2015). This allowed statistical comparisons, based on 95% confidence intervals, for each layer, zone and pH.

Results

Seawater parameters

Mean seawater carbonate chemistry parameters are presented in Table 2. Seawater temperature followed natural variations and ranged from 12.6 °C ± 0.7 °C at the start of the experimental period (in February) to 16.5 °C ± 0.5 °C at the end (in June/July). Salinity was 34.6 ± 0.6 in all experimental aquaria and remained stable over the experiment. Total alkalinity (A_T) measured in the experimental tanks was 2355 ± 9 µEq. kg^{-1} and remained stable over the experiment and between all aquaria. The pH_T in aquaria was maintained closed to nominal value along the experiment, with 8.01 ± 0.05 (pCO_2 439 ± 57 µatm) in control aquaria and 7.71 ± 0.06 (pCO_2 951 ± 138 µatm) in lower pH aquaria. $\Omega_{aragonite}$ was 2.30 ± 0.31 and 1.25 ± 0.19 and $\Omega_{calcite}$ was 3.59 ± 0.46 and 1.95 ± 0.28 in pH 8.0 and pH 7.7 conditions, respectively.

Table 2. Seawater temperature, salinity and parameters of the carbonate system in each pH treatment (i.e., pH 8.0 and pH 7.7, n = 5 per treatment). Seawater pH on the total scale (pH_T), temperature, salinity and total alkalinity (mean 2355 ± 9 µEq. kg^{-1}) were used to calculate CO_2 partial pressure (pCO_2; µatm), dissolved inorganic carbon (DIC; µmol/kg), HCO_3^- (µmol/kg), CO_3^{2-} (µmol/kg), aragonite saturation state (Ω_{ar}) and calcite saturation state (Ω_{calc}) by using the CO_2SYS program. Values are means ± SD.

Carbonate system parameter	pH 8.0	pH 7.7
Nominal pH	8.0	7.7
pH_T	8.01 ± 0.05	7.71 ± 0.06
Temperature (°C)	14.4 ± 1.4	14.4 ± 1.5
Salinity	34.6 ± 0.6	34.6 ± 0.6
pCO_2 (µatm)	439 ± 57	951 ± 138
DIC (µmol/kg)	2150 ± 28	2277 ± 25
HCO_3^- (µmol/kg)	1984 ± 48	2154 ± 30
CO_3^{2-} (µmol/kg)	151 ± 20	82 ± 12
$\Omega_{aragonite}$	2.30 ± 0.31	1.25 ± 0.19
$\Omega_{calcite}$	3.59 ± 0.46	1.95 ± 0.28

Survival, biometry and growth

Abalone survival after five months of exposure to lowered pH was very high with no difference between individuals exposed to pH 8.0 and pH 7.7 (96.9 % and 95.4 %, respectively, Table 3).

At M5, abalone exposed to pH 8.0 grew at a rate of 0.039 ± 0.003 mm/day while the growth rate of those exposed to pH 7.7 was significantly lower, at 0.027 ± 0.003 mm/day (Figure 2a, Table 3). No differences in growth rate were observed at earlier sampling times (Table 3).

After two months of pH exposure at the two levels, specific growth rate was lower for abalone exposed to pH 8.0 compared with abalone exposed to pH 7.7 (Table 3, Figure 2b). No significant differences in specific growth rate were observed at M3 and M4 between the control and low pH groups.

No significant difference was observed for the haemolymph or muscle weights (Table 3). However, at M4, the gonad weight was significantly lower for individuals exposed to pH 7.7. (1.38 ± 0.14 g, Table 3) compared with those exposed to pH 8.0 (1.75 ± 0.13 g).

Table 3. Summary of mixed model results used to test the effect of pH on studied parameters in adult abalone (pH: fixed factor, tank: random factor) after one week (W1), two (M2), three (M3), four (M4) and five (M5) months of exposure. A Welch's Heteroscedastic F (1) or a Student-t (2) test was used when necessary. Significant results are shown in bold ($p < 0.05$).

Parameter	W1	M2	M3	M4	M5
Survival	----------	----------	----------	----------	t_{258}=-0.64, p=0.521 (2)
Shell growth in length	----------	$F_{1,36}$=2.11, p=0.155	$F_{1,26}$=0.20, p=0.655	$F_{1,34}$=0.03, p=0.866	**$F_{1,8}$=7.25, p=0.027**
Specific growth rate	----------	**$F_{1,24}$=4.77, p=0.039**	$F_{1,24}$=0.39, p=0.539	$F_{1,7}$=0.02, p=0.887	----------
Haemolymph weight	$F_{1,9}$=4.01, p=0.078	$F_{1,10}$=1.39, p=0.267	$F_{1,24}$=3.98, p=0.058	$F_{1,7}$=0.41, p=0.544	----------
Muscle weight	$F_{1,14}$=0.02, p=0.905	$F_{1,34}$=1.12, p=0.298	$F_{1,8}$=3.64, p=0.091	$F_{1,43}$=0.54, p=0.467	----------
Gonad weight	$F_{1,15}$=0.26, p=0.619	$F_{1,33}$=0.07, p=0.793	$F_{1,24}$=2.19, p=0.152	**$F_{1,8}$=5.84, p=0.043**	----------
Haemolymph pH_T	**$F_{1,8}$=11.77, p=0.009**	**$F_{1,8}$=21.67, p=0.002**	----------	$F_{1,8}$=4.63, p=0.064	----------
Phagocytosis efficiency	$F_{1,8}$=0.07, p=0.802	$F_{1,8}$=0.89, p=0.373	----------	$F_{1,5}$=0.57, p=0.484 (1)	----------
Respiration rate	$F_{1,8}$=0.52, p=0.493	$F_{1,8}$=0.05, p=0.827	$F_{1,25}$=0.99, p=0.328	----------	----------
Excretion rate	$F_{1,6}$=0.34, p=0.582 (1)	$F_{1,4}$=1.75, p=0.253 (1)	$F_{1,9}$=0.04, p=0.849	----------	----------
Gene expression: Lustrin A	----------	----------	----------	$F_{1,6}$=0.66, p=0.446	----------
Gene expression: HSP71	----------	----------	----------	$F_{1,6}$=0.72, p=0.429 (1)	----------
Gene expression: HSP84	----------	----------	----------	$F_{1,7}$=0.10, p=0.757	----------
Gene expression: CA 1	----------	----------	----------	$F_{1,26}$=0.06, p=0.802	----------
Gene expression: CA 2	----------	----------	----------	$F_{1,5}$=2.49, p=0.178 (1)	----------
Shell coloration	$F_{1,8}$=3.28, p=0.107	**$F_{1,8}$=49.83, p<0.001**	**$F_{1,8}$=52.51, p<0.001**	**$F_{1,8}$=51.58, p<0.001**	**$F_{1,9}$=172.10, p<0.001**
Net calcification rate	**$F_{1,27}$=7.83, p=0.009**	$F_{1,8}$=0.33, p=0.582	**$F_{1,25}$=12.78, p=0.001**	----------	----------
Shell weight	$F_{1,43}$=0.01, p=0.913	$F_{1,9}$=2.49, p=0.149	$F_{1,24}$=3.59, p=0.070	$F_{1,30}$=0.46, p=0.501	$F_{1,8}$=4.81, p=0.059
Shell thickness	$F_{1,8}$=1.49, p=0.257	$F_{1,36}$=0.27, p=0.608	$F_{1,8}$=3.30, p=0.106	$F_{1,35}$=0.04, p=0.844	$F_{1,7}$=3.54, p=0.099
Periostracum thickness	----------	----------	----------	**$F_{1,5}$=28.84, p=0.002**	----------
Spherulitic layer thickness	----------	----------	----------	$F_{1,8}$=6.10^{-4}, p=0.982	----------
Nacre layer thickness	----------	----------	----------	$F_{1,8}$=0.08, p=0.785	----------
Platelet thickness	----------	----------	----------	t_4=-0.64, p=0.556 (2)	----------
Shell fracture force	----------	----------	----------	**$F_{1,18}$=6.53, p=0.020**	----------

408

409

410 ***Physiology and metabolism***

411 The pH_T of haemolymph in abalone exposed to pH 7.7 was significantly lower than those
412 exposed to pH 8.0 at W1 and M2 and a non-significant decrease was observed at M4 (Table 3,
413 Figure 3).

414 The phagocytosis efficiency was 33.3 ± 3.8 and 31.9 ± 3.8 % at W1, 33.6 ± 3.6 and 38.4 ± 3.6
415 % at M2, 13.9 ± 3.5 and 10.2 ± 3.5 % at M4 for individuals exposed to pH 8.0 and pH 7.7,
416 respectively. The phagocytosis efficiency of abalone haemocytes was not significantly
417 impacted by low pH at W1, M2 and M4 (Table 3).

418 No significant difference in respiration or excretion rates were observed between the two pH
419 treatments at any sampling time (Table 3). At the last point of measurement (M3), respiration
420 rates were -3.29 ± 0.13 and -3.11 ± 0.12 µmol O_2 $g^{-1}.h^{-1}$ and excretion rates were 0.05 ± 0.06
421 and 0.02 ± 0.02 µmol NH_4 $g^{-1}.h^{-1}$, respectively for individuals exposed to pH 8.0 and pH 7.7.

422 ***Gene expression***

423 No significant difference in gene expression was observed between the two pH treatments for
424 all tested genes at M4 (Table 3, Figure 4).

425 ***Shell pattern***

426 Periostracum of abalone exposed to pH 7.7 were lighter than those exposed to pH 8.0 (Figure
427 5a, b).The periostracum of abalone exposed to low pH had a significantly paler colour than
428 those of abalone exposed to pH 8.0, with darker coloration from M2 to M5 (Table 3, Figure
429 5c).

SEM examination of abalone shell surfaces exposed to pH 8.0 and pH 7.7 at M4 revealed differences in the texture and organization of outer and inner surface layers. The periostracum of control abalone (pH 8.0) had a homogeneous texture and regular organic sheets (Figure 6a, 6c). In contrast, the periostracum of individuals exposed to low pH (7.7) had an irregular and corroded surface (Figure 6b, 6d), revealing biominerals characteristic of the underlying spherulitic layer (Figure 6e).

The inner nacreous layer showed a progressive maturation of aragonite platelets, forming a smooth homogeneous surface in individuals exposed to the two pH treatments (Figure 7a - 7d). At a higher magnification, the nacre growth region of control shell exhibited regular aragonite platelets joining progressively (Figure 7e). In abalone shell exposed to pH 7.7, the nacre surface of the growth region appeared corroded, with evidence of dissolution of the aragonite platelets (Figure 7f).

Shell calcification

Net calcification rate measured in individuals exposed to pH 7.7 was significantly lower than in those exposed to pH 8.0 at W1 and M3 (Table 3, Figure 8).

No significant differences were observed in shell weight and shell thickness between the two pH treatments at any sampling time (Table 3).

At M4, a significant thinner periostracum was observed for abalone exposed to pH 7.7 compared with those exposed to pH 8.0 (Table 3, Figure 9). The thickness of the spherulitic and nacre layers did not differ between the individuals exposed to the two pH treatments (Table 3, Figure 9).

At M4, cross-sections in the newly formed shell (Figure 10a, 10b) revealed the distinction between the spherulitic and nacreous layers, both for individuals exposed to pH 8.0 (Figure 10c) and those exposed to pH 7.7 (Figure 10d). Magnification of the nacre platelets in cross-

section revealed irregularities with a heterogeneous and corroded texture in the abalone exposed to pH 7.7 (Figure 10f) compared with those exposed to pH 8.0 (Figure 10e). In addition, the interspace between the aragonite platelets appeared reduced, resulting in a more tightly packed nacre layer in pH 7.7 (Figure 10e). No significant difference was observed in the thickness of nacreous tablets in the recent deposited nacre in abalone exposed to low pH at M4 compared with control abalone (0.42 ± 0.07 µm vs 0.39 ± 0.07 µm respectively, Table 3); or in the older part of the shell (0.39 ± 0.03 µm vs 0.44 ± 0.04 µm respectively, Table 3).

At M4, the shell fracture force was significantly lower for abalone shells exposed to pH 7.7 compared with the pH 8.0 control group (200 ± 70 N and 281 ± 71 N respectively, Table 3). No linear relationship was found between the shell fracture force and shell length (Linear regression, $R^2 = 0.037$, $F_{1,18} = 0.71$, $p = 0.412$), shell weight (Linear regression, $R^2 = 0.130$, $F_{1,18} = 2.70$, $p = 0.118$), shell area (Linear regression, $R^2 = 0.112$, $F_{1,17} = 2.15$, $p = 0.161$) or shell thickness (Linear regression, $R^2 = 0.024$, $F_{1,16} = 0.39$, $p = 0.542$).

Weibull analysis of the characteristic Young's modulus E_0 obtained by nanoindentation revealed that Young's modulus of elasticity was significantly lower in the external layer than in the nacre (Supplementary Table S2). It also indicated that at pH 8.0 E_0 did not significantly differ according to zones (old, intermediate, newly formed) in the external layer and only slightly differed according to the zones in the nacre, the intermediate zone E_0 being significantly different from that of the old zone (Figure 11, Supplementary Table S2). On the contrary, under low pH, the E_0 values differed significantly according to zone (Figure 11, Supplementary Table S2). Furthermore, the analysis revealed that the shells of abalone exposed to low pH had a lower Young's modulus of elasticity. This was true for each layer (external layer and nacre) and for each zone (old, intermediate and newly formed) with the exception of the old zone of the external layer whose E_0 did not differ according to pH (Figure 11, Supplementary Table S2).

Weibull analysis of characteristic nanohardness (H_0) revealed similar changes as for E_0. At pH 8.0, H_0 did not differ according to zones in the external layer and was only slightly (but significantly) higher in the old nacre zone than in the two other zones of this layer. H_0 was significantly lower at pH 7.7 than at pH 8.0, except in the newly formed zone of the external layer and in the intermediate layer of the nacre (Figure 11, Supplementary Table S3).

Discussion

This study used a multifactorial approach to investigate several biological (including survival and growth reported as length), physiological (including pH_T of haemolymph, gene expression relating to calcification and metabolic rates) and structural (including shell strength, nanoindentation measurements, SEM imaging of microstructure) responses in adult abalone *H. tuberculata* exposed to decreased pH. A number of biological parameters involved in shell calcification, as growth, shell strength or microstructure, and acid-base regulation, as pH_T of haemolymph, were reduced at pH 7.7, while survival, metabolism and haemocyte phagocytosis were not significantly affected.

A significant effect of OA was observed on several biological responses including shell growth of adult abalone in terms of length after five months of low pH exposure, which is in accordance with previous studies on juvenile abalone. Indeed, Cunningham *et al.* (2016) reported significant reductions in shell length and weight in juveniles *H. iris* exposed to low pH (-0.3 to -0.5 pH units from ambient pH). Similarly, reduced shell growth in length under acidified pH conditions have recently been reported in six-month-old juvenile *H. tuberculata* exposed to pH 7.6 (Auzoux-Bordenave *et al.*, 2019). Although there are no studies available on adult abalone, our results are consistent with previous research showing a shell growth reduction in almost all mollusc taxa exposed to OA (Gazeau *et al.*, 2013; Kroeker *et al.*, 2013)

503 but with differences according to life stage. For example, adult snails *Nucella lamellosa*
504 exposed to acidified conditions (-0.2 and -0.4 pH units from ambient pH) showed a decline in
505 shell growth due to an increased dissolution of shell material (Nienhuis *et al.*, 2010).
506 Significant growth reductions are regularly observed in juveniles exposed to acidified
507 conditions (Michaelidis *et al.*, 2005; Beniash *et al.*, 2010; Thomsen and Melzner, 2010;
508 Amaral *et al.*, 2012), but the magnitude of the effect is generally smaller in adults, where the
509 calcification is lower.

510 In adult *H. tuberculata*, no significant differences in shell weight and shell thickness were
511 found between the two pH treatments. However, after four months under low pH exposure,
512 abalone shells showed a corroded and disorganized periostracum which was associated to
513 changes in shell coloration. The periostracum plays a role in maintaining shell integrity in
514 acidified seawater conditions (Ries *et al.*, 2009), protecting individuals from dissolution in
515 $CaCO_3$-undersaturated waters (Hüning *et al.*, 2012). In our study, the periostracum appeared
516 clearly corroded under lower pH, showing biominerals emerging from the underlying
517 spherulitic layer. This was confirmed by a significant reduction of the periostracum thickness.
518 These observations are consistent with previous observations relating prominent dissolution
519 on the outer surface of juvenile abalone and other mollusc shells (Mac Clintok *et al.*, 2009;
520 Meng *et al.*, 2018; Auzoux-Bordenave *et al.*, 2019). In addition, corrosion of aragonite
521 platelets and surface dissolution were observed within the nacreous inner layer of the shell
522 from individuals exposed to pH 7.7. No significant differences were observed in the thickness
523 of the spherulitic layer which is just beneath the periostracum. As previously seen in juvenile
524 stage of *H. tuberculata* (Auzoux-Bordenave *et al.*, 2019), these observations suggest a
525 reduction in shell protection from environmental disturbances and also from potential
526 predators in adult abalone.

Although no significant differences in nacre thickness were found, the decrease of -0.3 pH units resulted in a partial dissolution of nacreous surface. The nacre surface dissolution is consistent with the effects observed on juvenile abalone and adult bivalve shells grown at similar levels of pH treatments (Mac Clintok *et al.,* 2009; Thomsen *et al*., 2010; Welladsen *et al.*, 2010; Melzner *et al.,* 2011; Auzoux-Bordenave *et al.*, 2019). In juvenile *Mytilus edulis*, the aragonite layer was more vulnerable than the calcite layer under low pH (-0.8 pH units from ambient), with a corroded and dissolved surface (Thomsen *et al.*, 2010; Melzner *et al.*, 2011). The growth of new nacre tablets was also disrupted in adult pearl oysters *Pinctada fucata* kept at pH 7.6, as the developing tablets were deformed and irregular (Welladsen *et al.*, 2010). In *H. tuberculata* nacre, we also evidenced a reduction of the inter-tabular space within the aragonite platelets, resulting in a more tightly packed nacre layer in pH 7.7. The tight packing of nacre platelets under lower pH suggests changes in the structural organization of organic matrix surrounding the platelets. This might be further explored by combining high-resolution TEM and electron energy loss spectroscopy (EELS) to gain local information and detect fine changes in the organo-mineral interface.

In *H. tuberculata*, the main $CaCO_3$ polymorph composing the shell is aragonite (Auzoux-Bordenave *et al.*, 2010; Auzoux-Bordenave *et al.*, 2015), indicating that this species is more susceptible to dissolution than other mollusc shells composed of only calcite or a mixture of calcite/aragonite (Gazeau *et al.*, 2013; Parker *et al.*, 2013). The formation of calcified layers is strongly impacted when the saturation state of aragonite in seawater is < 1 (Comeau *et al.*, 2010; Gazeau *et al.*, 2013). Since the aragonite saturation state ($\Omega_{aragonite}$) of the seawater was always > 1 in our study, the shells effects might not be entirely due to shell dissolution. It is suggested that indirect metabolic effects, such as disruption of the acid-base balance, would be partly responsible for shell corrosion and microstructure changes observed under lower pH. In our study, net calcification of adult abalone was significantly decreased at lower pH (7.7),

552 which is a common response in molluscs (Beniash *et al.*, 2010; Range *et al.*, 2011; Melatunan
553 *et al.*, 2013). Indeed, previous studies on temperate bivalves exposed to acidified seawater
554 have shown reduced calcification rates that would compromise the structural integrity of the
555 shell (Michaelidis *et al.*, 2005; Gazeau *et al.*, 2007; Ries *et al.*, 2009; Beniash *et al.*, 2010;
556 Range *et al.*, 2011). On adult slipper limpet, *Crepidula fornicata*, negative calcification rates
557 in individuals exposed to very low pH (-0.5 pH units) were correlated with a degraded
558 periostracum and/or physiological changes (Noisette *et al.*, 2016). The alteration of the
559 periostracum and corrosion of the nacreous layer observed in abalone shells may be partly
560 explained by a reduced calcification rate.

561 Previous experimental studies on OA reported that a reduction in shell structural integrity
562 induced significant reduction in mechanical properties (Beniash *et al.*, 2010; Dickinson *et al.*,
563 2012; Fitzer *et al.*, 2015). Our study investigated for the first time the impacts of OA on the
564 biomechanical properties of adult abalone shell. The shell fracture force was significantly
565 reduced after four months of exposure to acidified seawater. This result is consistent with the
566 changes in shell microstructure observed under SEM. In juvenile *H. tuberculata* shell, the
567 reduction of shell fracture force under low pH (pH 7.6) resulted from both reduced growth
568 and shell dissolution (Auzoux-Bordenave *et al.*, 2019). At the adult stage, the fracture force of
569 abalone shells exposed to pH 7.7 was reduced by 29 % compared with the control, indicating
570 that defects induced by OA in adult shells are more severe than those induced in the juvenile
571 ones. Indeed, significantly lower elasticity and hardness were observed in the newly formed
572 shell of abalone exposed to acidified seawater. By contrast, values for the oldest part of the
573 shell were similar to those recorded in the shells of abalone exposed to pH 8.0. This suggest
574 that the synthesis of new shell is the affected process, rather than corrosion (which impacted
575 the whole shell surface). These results also indicate that the material properties themselves are
576 affected in both the nacre and spherulitic layers and that this induced mechanical weakness of

577 the shell. Similar results were reported in *M. edulis* (Fitzer *et al.*, 2015) but this is, to our
578 knowledge, the first evidence in gastropods, suggesting that the shell formation process is
579 affected differently among mollusc clades.

580 Along with direct impacts on calcification, exposure to low pH seawater may also have
581 indirect effects on the extracellular acid-base equilibrium, leading to general internal acidosis,
582 changes in energy balance and disruption in shell calcification (Pörtner *et al.*, 2004; Melzner
583 *et al.*, 2009; Waldbusser *et al.*, 2011). The multifactorial approach used in this study also
584 allowed the assessment of acid-base, metabolism and physiology parameters in adult abalone
585 *H. tuberculata* facing OA. A decrease in haemolymph pH was observed under lower pH
586 during the first two months of exposure, indicating a lack of compensation in abalone facing
587 OA. Elevated H^+ concentration and subsequent changes in acid-base balance would likely be
588 responsible for the reduction of shell calcification in marine molluscs (Waldbusser *et al.*,
589 2011; Cyronak *et al.*, 2016). Furthermore, an increased cost for ion regulation combined with
590 decreased growth could lead to a lower rate of calcification (Pörtner *et al.*, 2004; Michaelidis
591 *et al.*, 2005). In the present study, we demonstrated that adult *H. tuberculata* do not
592 compensate for a seawater pH decrease of 0.3 pH units, suggesting that changes in the
593 extracellular balance might be partly responsible for the alteration of shell integrity.

594 Among the physiological processes involved in shell calcification, matrix protein production
595 and specific enzymatic activities (i.e., carbonic anhydrase) have been shown to be influenced
596 by decreased pH (Weiss *et al.*, 2013). Our study also investigated the expression of five genes
597 involved in abalone shell biomineralization (Lustrin A, CA1 and CA2) and stress response
598 (HSP70 and HSP84). Despite evidence of shell damage, no difference was found in the
599 expression of the biomineralization genes nor in genes involved in stress responses. The
600 activity of carbonic anhydrase (CA), which plays a major role in the formation of carbonate
601 ions, was significantly reduced in adult *M. edulis* exposed to a similar pH decrease (Fitzer *et*

602 *al.*, 2014). However, in this study, only CA activity was measured and gene expression was
603 not evaluated. An increase of HSP gene expression has been previously reported in mollusc
604 exposed either to thermal stress (Farcy *et al.*, 2007) or to lower pH (Cummings *et al.*, 2011).
605 In the present study on *H. tuberculata*, we did not find any change in the expression of target
606 genes, suggesting that the physiological responses to OA would occur at another level of
607 regulation such as protein synthesis or structural organisation. As already performed in *H.*
608 *rufescens* (De Wit and Palumbi, 2013), future works would likely include a complete
609 transcriptome analysis in the mantle of *H. tuberculata* in order to identify the molecular
610 responses of European abalone to OA.

611 OA may also impact the physiological status and functionality of the haemocytes, as
612 previously shown in *M. edulis* (Bibby *et al.*, 2008). In adult abalone *H. tuberculata*, the
613 immune response, evaluated by haemocyte phagocytosis, was not significantly affected by
614 lowered pH, regardless of the sampling time. In addition, no significant changes were
615 observed in global metabolism (respiration and excretion rates) between animals in the
616 control treatment and those at lowered pH. This is consistent with previous results on
617 calcifying molluscs showing that metabolism was only slightly increased among adult
618 individuals (reviewed in Kroeker *et al.,* 2013). The absence of significant effects on abalone
619 metabolism is also in accordance with the results obtained on juvenile *H. iris* (Cunningham *et*
620 *al.*, 2016) and adult *C. fornicata* (Noisette *et al.*, 2016). The capacity of abalone to grow
621 under future pH conditions will depend on their potential to maintain their vital functions.
622 Since the seawater pH along the Brittany coast naturally varies from 7.9 to 8.2 (Legrand *et al.*,
623 2018; Qui-Minet *et al.*, 2018), the experimental scenario testing a decrease of -0.3 units from
624 ambient pH is consistent with natural variations experienced by abalone in the tidal zone.

625 From these results, it was concluded that European abalone *H. tuberculata* did not
626 compensate the decrease of seawater pH (-0.3 pH units) during the first two months of

627 exposure, but started to acclimate after four months, as suggested by the compensation of
628 their extracellular pH. After four months of exposure under low pH, the acid-base balance and
629 global metabolism were not affected by OA, but occurred at a cost to shell growth and
630 structural integrity. Indeed, adverse effects on shell growth, calcification and mechanical
631 properties were observed, supporting the idea that OA altered the biomineral architecture and
632 lead to more fragile shell. These effects are of particular concern in this economically and
633 ecologically important abalone species. The decrease in shell resistance might reduce
634 protection from predators and potentially impact wild abalone populations already threatened
635 by overfishing and environmental perturbations (Cook, 2016). This effect adds to the
636 increased mortality and reduced growth already reported in larvae and juvenile of *H.*
637 *tuberculata* for pH of 7.6 (Wessel *et al.*, 2018; Auzoux-Bordenave *et al.*, 2019). Because
638 abalone are slow growing species, the impact of a decreased pH during the aquaculture cycle
639 might substantially increase production costs by increasing the time necessary for animals to
640 reach a marketable size.

641

642 **Supplementary material**

643 Supplementary material is available at the *ICESJMS* online version of the manuscript.

644

645 **Acknowledgements**

646 This work was supported in part by the ATM program "Abalone shell mineralization" of the
647 MNHN funded by the *Ministère délégué à l'Enseignement Supérieur et à la Recherche* (Paris,
648 France), the program "*Acidification des Océans*" (ICOBio project) funded by the *Fondation*
649 *pour la Recherche sur la Biodiversité* (FRB) and the *Ministère de la Transition Ecologique et*
650 *Solidaire* (MTES), and the French LabexMER program (OASYS project). SA was supported

by a post-doctoral fellowship from the MNHN funded by the *Ministère de la Transition Ecologique et Solidaire* (MTES). SdG is holder of a FRIA PhD fellowship from the National Fund for Scientific Research (NFSR, Belgium) and PhD is a Research Director of the NFSR. The Regional Council of Brittany, the General Council of Finistère, the urban community of Concarneau Cornouaille Agglomération and the European Regional Development Fund (ERDF) are acknowledged for the funding of the scanning electron microscope (Sigma 300 FE-SEM) at the Concarneau Marine Station. We thank Stéphane Formosa for his assistance in SEM (*Plateau technique de Microscopie Electronique du Muséum National d'Histoire Naturelle,* Concarneau, France). We are grateful to Olivier Mouchel for his help in sampling abalone and Nicolas Brodu who participated to the experimental work and biological analyses during his master training. We thank all the staff of the France Haliotis farm (Plouguerneau) for hosting the experiment. Finally, we thank the Translation Bureau of the University of Western Brittany for improving the English of this manuscript.

Authors' contributions

S.A.-B., S.M., S.R. and Ph.D. designed the experiment; M.C., S.R., A.B. and S.H. performed the experiment; S.H. provided the facilities; N.R., S.d G., L.M. and Ph.D. performed the mechanical analysis and the data analysis; A.S and F.G. performed the gene expression analysis; S.A., S.R. and S.A.-B. analysed the data and wrote the main paper. All authors discussed the results and implications and commented on the manuscript at all stages.

References

Amaral, V., Cabral, H., and Bishop, M. 2012. Moderate acidification affects growth but not survival of 6-month-old oysters. Aquatic ecology, 46: 119–127.

675 Auzoux-Bordenave, S., Badou, A., Gaume, B., Berland, S., Helléouet, M. N., Milet, C., and
676 Huchette, S. 2010. Ultrastructure, chemistry and mineralogy of the growing shell of
677 the European abalone *Haliotis tuberculata*. Journal of Structural Biology, 171: 277–
678 290.
679 Auzoux-Bordenave, S., Brahmi, C., Badou, A., De Rafélis, M., and Huchette, S. 2015. Shell
680 growth, microstructure and composition over the development cycle of the European
681 abalone *Haliotis tuberculata*. Marine Biology, 162: 687–697.
682 Auzoux-Bordenave, S., Wessel, N., Badou, A., Martin, S., M'Zoudi, S., Avignon, S., Roussel,
683 S., Huchette, S. and Dubois, P. 2019. Ocean acidification impacts growth and shell
684 mineralization in juvenile abalone (*Haliotis tuberculata*), Marine Biology, in press.
685 Beniash, E., Ivanina, A., Lieb, N. S., Kurochkin, I., and Sokolova, I. M. 2010. Elevated level
686 of carbon dioxide affects metabolism and shell formation in oysters *Crassostrea*
687 *virginica*. Marine Ecology Progress Series, 419: 95–108.
688 Bibby, R., Widdicombe, S., Parry, H., Spicer, J., and Pipe, R. 2008. Effects of ocean
689 acidification on the immune response of the blue mussel *Mytilus edulis*. Aquatic
690 Biology, 2: 67–74.
691 Bütikofer, L., Stawarczyk, B., and Roos, M. 2015. Two regression methods for estimation of
692 a two-parameter Weibull distribution for reliability of dental materials. Dental
693 Materials, 31: e33–e50.
694 Cadiz, L., Servili, A., Quazuguel, P., Madec, L., Zambonino-Infante, J.-L., and Mazurais, D.
695 2017. Early exposure to chronic hypoxia induces short- and long-term regulation of
696 hemoglobin gene expression in European sea bass (*Dicentrarchus labrax*). The
697 Journal of Experimental Biology, 220: 3119–3126.
698 Caldeira, K., and Wickett, M. E. 2003. Anthropogenic carbon and ocean pH. Nature, 425:
699 365.
700 Comeau, S., Gorsky, G., Alliouane, S., and Gattuso, J. P. 2010. Larvae of the pteropod
701 *Cavolinia inflexa* exposed to aragonite undersaturation are viable but shell-less.
702 Marine Biology, 157: 2341–2345.
703 Cook, P. A. 2016. Recent trends in worldwide abalone production. Journal of Shellfish
704 Research, 35: 581–583.
705 Cummings, V., Hewitt, J., Van Rooyen, A., Currie, K., Beard, S., Thrush, S., Norkko, J., *et al.*
706 2011. Ocean acidification at high latitudes: potential effects on functioning of the
707 antarctic bivalve *Laternula elliptica*. PLOS ONE, 6.

708 Cunningham, S. C., Smith, A. M., and Lamare, M. D. 2016. The effects of elevated pCO_2 on
709 growth, shell production and metabolism of cultured juvenile abalone, *Haliotis iris*.
710 Aquaculture Research, 47: 2375–2392.
711 Cyronak, T., Schulz, K. G., and Jokiel, P. L. 2016. The Omega myth: what really drives lower
712 calcification rates in an acidifying ocean. ICES Journal of Marine Science, 73: 558–
713 562.
714 De Wit, P., and Palumbi, S. R. 2013. Transcriptome-wide polymorphisms of red abalone
715 (*Haliotis rufescens*) reveal patterns of gene flow and local adaptation. Molecular
716 Ecology, 22: 2884–2897.
717 Dickinson, G. H., Ivanina, A. V., Matoo, O. B., Portner, H. O., Lannig, G., Bock, C., Beniash,
718 E., *et al.* 2012. Interactive effects of salinity and elevated CO_2 levels on juvenile
719 eastern oysters, *Crassostrea virginica*. Journal of Experimental Biology, 215: 29–43.
720 Dickson, A. G., and Millero, F. J. 1987. A comparison of the equilibrium constants for the
721 dissociation of carbonic acid in seawater media. Deep-Sea Research, 34: 1733–1743.
722 Dickson, A. G., Sabine, C. L., and Christian, J. R. (Eds). 2007. Guide to best practices for
723 ocean CO_2 measurements. PICES Special Publication. 191 pp.
724 Dickson, A. G. 2010. Standards for ocean measurements. Oceanography, 23: 34–47.
725 Fabry, V. J. 2008. Marine calcifiers in a high-CO_2 ocean. Science, 320: 1020–1022.
726 Farcy, E., Serpentini, A., Fiévet, B., and Lebel, J.-M. 2007. Identification of cDNAs encoding
727 HSP70 and HSP90 in the abalone *Haliotis tuberculata*: Transcriptional induction in
728 response to thermal stress in hemocyte primary culture. Comparative Biochemistry
729 and Physiology Part B: Biochemistry and Molecular Biology, 146: 540–550.
730 Fitzer, S. C., Phoenix, V. R., Cusack, M., and Kamenos, N. A. 2014. Ocean acidification
731 impacts mussel control on biomineralisation. Scientific Reports, 4: 6218.
732 Fitzer, S. C., Zhu, W., Tanner, K. E., Phoenix, V. R., Kamenos, N. A., and Cusack, M. 2015.
733 Ocean acidification alters the material properties of *Mytilus edulis* shells. Journal of
734 the Royal Society Interface, 12: 20141227.
735 Gattuso, J. P., Magnan, A., Bille, R., Cheung, W. W. L., Howes, E. L., Joos, F., Allemand, D.,
736 *et al.* 2015. Contrasting futures for ocean and society from different anthropogenic
737 CO_2 emissions scenarios. Science, 349: 4722–4722.
738 Gaume, B., Denis, F., Van Wormhoudt, A., Huchette, S., Jackson, D. J., Avignon, S., and
739 Auzoux-Bordenave, S. 2014. Characterisation and expression of the biomineralising
740 gene Lustrin A during shell formation of the European abalone *Haliotis tuberculata*.

741 Comparative Biochemistry and Physiology Part B: Biochemistry and Molecular
742 Biology, 169: 1–8.
743 Gazeau, F., Quiblier, C., Jansen, J. M., Gattuso, J.-P., Middelburg, J. J., and Heip, C. H. R.
744 2007. Impact of elevated CO_2 on shellfish calcification. Geophysical Research Letters,
745 34: L07703.
746 Gazeau, F., Parker, L. M., Comeau, S., Gattuso, J.-P., O'Connor, W. A., Martin, S., Pörtner,
747 H.-O., *et al.* 2013. Impacts of ocean acidification on marine shelled molluscs. Marine
748 Biology, 160: 2207–2245.
749 Hendriks, I. E., Duarte, C. M., and Álvarez, M. 2010. Vulnerability of marine biodiversity to
750 ocean acidification: A meta-analysis. Estuarine, Coastal and Shelf Science, 86: 157–
751 164.
752 Hoegh-Guldberg, O., Mumby, P. J., Hooten, A. J., Steneck, R. S., Greenfield, P., Gomez, E.,
753 Harvell, C. D., *et al.* 2007. Coral reefs under rapid climate change and ocean
754 acidification. Science, 318: 1737.
755 Hofmann, G. E., Barry, J. P., Edmunds, P. J., Gates, R. D., Hutchins, D. A., Klinger, T., and
756 Sewell, M. A. 2010. The effect of ocean acidification on calcifying organisms in
757 marine ecosystems: An organism-to-ecosystem perspective. Annual Review of
758 Ecology, Evolution and Systematics, 41: 127–147.
759 Huchette, S., and Clavier, J. 2004. Status of the ormer (*Haliotis tuberculata* L.) industry in
760 Europe. Journal of Shellfish Research, 23: 951–955.
761 Hüning, A. K., Melzner, F., Thomsen, J., Gutowska, M. A., Krämer, L., Frickenhaus, S.,
762 Rosenstiel, P., *et al.* 2012. Impacts of seawater acidification on mantle gene
763 expression patterns of the Baltic Sea blue mussel: Implications for shell formation and
764 energy metabolism. Marine Biology, 160: 1845–1861.
765 IPCC. 2014. Summary for Policymakers. *In* Climate Change 2014: Impacts, Adaptation, and
766 Vulnerability. Part A: Global and Sectoral Aspects. Contribution of Working Group II
767 to the Fifth Assessment Report of the Intergovernmental Panel on Climate Change, pp.
768 1–32. Cambridge University Press, Cambridge, United Kingdom and New York, NY,
769 USA.
770 Kroeker, K. J., Kordas, R. L., Crim, R., Hendriks, I. E., Ramajo, L., Singh, G. S., Duarte, C.
771 M., *et al.* 2013. Impacts of ocean acidification on marine organisms: quantifying
772 sensitivities and interaction with warming. Global Change Biology, 19: 1884–1896.
773 Kuznetsova, A., Brockhoff, P. B., and Christensen, R. H. B. 2017. lmerTest package: Tests in
774 linear mixed effects models. Journal of Statistical Software, 82: 1–26.

775 Le Roy, N., Marie, B., Gaume, B., Guichard, N., Delgado, S., Zanella-Cléon, I., Becchi, M.,
776 *et al.* 2012. Identification of two carbonic anhydrases in the mantle of the European
777 abalone *Haliotis tuberculata* (Gastropoda, Haliotidae): Phylogenetic implications.
778 Journal of Experimental Zoology Part B: Molecular and Developmental Evolution,
779 318: 353–367.
780 Legrand, E., Riera, P., Pouliquen, L., Bohner, O., Cariou, T., and Martin, S. 2018. Ecological
781 characterization of intertidal rockpools: Seasonal and diurnal monitoring of physico-
782 chemical parameters. Regional Studies in Marine Science, 17: 1–10.
783 Marchant, H. K., Calosi, P., and Spicer, J. I. 2010. Short-term exposure to hypercapnia does
784 not compromise feeding, acid–base balance or respiration of *Patella vulgata* but
785 surprisingly is accompanied by radula damage. Journal of the Marine Association of
786 the United Kingdom, 90: 1379–1384.
787 McClintock, J. B., Angus, R. A., Mcdonald, M. R., Amsler, C. D., Catledge, S. A., Vohra, Y.
788 K. 2009. Rapid dissolution of shells of weakly calcified Antarctic benthic
789 macroorganisms indicates high vulnerability to ocean acidification. Antarctic Science,
790 21:449–456.
791 Mehrbach, C., Culberson, C. H., Hawley, J. E., and Pytkowicx, R. M. 1973. Measurement of
792 the apparent dissociation constants of carbonic acid in seawater at atmospheric
793 pressure. Limnology and Oceanography, 18: 897–907.
794 Melatunan, S., Calosi, P., Rundle, S., Widdicombe, S., and Moody, A. 2013. Effects of ocean
795 acidification and elevated temperature on shell plasticity and its energetic basis in an
796 intertidal gastropod. Marine Ecology Progress Series, 472: 155–168.
797 Melzner, F., Gutowska, M. A., Langenbuch, M., Dupont, S., Lucassen, M., Thorndyke, M. C.,
798 Bleich, M., *et al.* 2009. Physiological basis for high CO_2 tolerance in marine
799 ectothermic animals: pre-adaptation through lifestyle and ontogeny? Biogeosciences,
800 6: 2313–2331.
801 Melzner, F., Stange, P., Trübenbach, K., Thomsen, J., Casties, I., Panknin, U., Gorb, S. N., *et*
802 *al.* 2011. Food supply and seawater pCO_2 impact calcification and internal shell
803 dissolution in the blue mussel *Mytilus edulis*. PLOS ONE, 6: e24223.
804 Meng, Y., Guo, Z., Fitzer, S. C., Upadhyay, A., Chan, V. B. S., Li, C., Cusack, M., *et al.*
805 2018. Ocean acidification reduces hardness and stiffness of the Portuguese oyster shell
806 with impaired microstructure: a hierarchical analysis. Biogeosciences, 15: 6833-6846.

807 Michaelidis, B., Ouzounis, C., Paleras, A., and Pörtner, H.-O. 2005. Effects of long-term
808 moderate hypercapnia on acid–base balance and growth rate in marine mussels
809 *Mytilus galloprovincialis*. Marine Ecology Progress Series, 293: 109–118.
810 Morash, A. J., and Alter, K. 2015. Effects of environmental and farm stress on abalone
811 physiology: Perspectives for abalone aquaculture in the face of global climate change.
812 Reviews in Aquaculture, 7: 1–27.
813 Morse, J. W., Arvidson, R. S., and Lüttge, A. 2007. Calcium carbonate formation and
814 dissolution. Chemical Reviews, 107: 342–381.
815 Nienhuis, S., Palmer, A. R., and Harley, C. D. G. 2010. Elevated CO_2 affects shell dissolution
816 rate but not calcification rate in a marine snail. Proceedings of the Royal Society B:
817 Biological Sciences, 277: 2553–2558.
818 Noisette, F., Bordeyne, F., Davoult, D., and Martin, S. 2016. Assessing the physiological
819 responses of the gastropod *Crepidula fornicata* to predicted ocean acidification and
820 warming. Limnology and Oceanography, 61: 430–444.
821 Orr, J. C., Fabry, V. J., Aumont, O., Bopp, L., Doney, S. C., Feely, R. A., Gnanadesikan, A.,
822 *et al.* 2005. Anthropogenic ocean acidification over the twenty-first century and its
823 impact on calcifying organisms. Nature, 437: 681–686.
824 Parker, L. M., Ross, P. M., O'Connor, W. A., Borysko, L., Raftos, D. A., and Pörtner, H.-O.
825 2012. Adult exposure influences offspring response to ocean acidification in oysters.
826 Global Change Biology, 18: 82–92.
827 Parker, L. M., Ross, P. M., O'Connor, W. A., Pörtner, H.-O., Scanes, E., and Wright, J. M.
828 2013. Predicting the response of molluscs to the impact of ocean acidification.
829 Biology, 2: 651–692.
830 Pierrot, D. E., Lewis, E., and Wallace, D. W. R. 2006. MS Excel program developed for CO_2
831 system calculations. ORNL/CDIAC-105a. Carbon Dioxide Information Analysis
832 Center. Oak Ridge National Laroratory, US Department of Energy, Oak Ridge,
833 Tennessee.
834 Pörtner, H. O., Langenbuch, M., and Reipschläger, A. 2004. Biological impact of elevated
835 ocean CO_2 concentrations: lessons from animal physiology and earth history. Journal
836 of Oceanography, 60: 705–718.
837 Qui-Minet, Z. N., Delaunay, C., Grall, J., Six, C., Cariou, T., Bohner, O., Legrand, E., *et al.*
838 2018. The role of local environmental changes on maerl and its associated non-
839 calcareous epiphytic flora in the Bay of Brest. Estuarine, Coastal and Shelf Science,
840 208: 140–152.

R Core Team. 2015. R Core Team: A language and environment for statistical computing. Vienna, Austria. https://www.R-project.org/.

Range, P., Chicharo, M. A., Ben-Hamadou, R., Pilo, D., Matias, D., Joaquim, S., Oliveira, A. P., *et al.* 2011. Calcification, growth and mortality of juvenile clams *Ruditapes decussatus* under increased pCO_2 and reduced pH: Variable responses to ocean acidification at local scales? Journal of Experimental Marine Biology and Ecology, 396: 177–184.

Ries, J. B., Cohen, A. L., and McCorkle, D. C. 2009. Marine calcifiers exhibit mixed responses to CO_2-induced ocean acidification. Geology, 37: 1131–1134.

Rogers-Bennett, L. 2007. Is climate change contributing to range reductions and localized extinctions in northern (*Haliotis kamtschatkana*) and flat (*Haliotis walallensis*) abalones? Bulletin of Marine Science, 81: 283–296.

Sabine, C. L., Feely, R. A., Gruber, N., Key, R. M., Lee, K., Bullister, J. L., Wanninkhof, R., *et al.* 2004. The oceanic sink for anthropogenic CO_2. Science, 305: 367–371.

Shen, X., Belcher, A. M., Hansma, P. K., Stucky, G. D., and Morse, D. E. 1997. Molecular cloning and characterization of Lustrin A, a matrix protein from shell and pearl nacre of *Haliotis rufescens*. The Journal of biological chemistry, 272: 32472–32481.

Smith, S. V., and Key, G. S. 1975. Carbon dioxide and metabolism in marine environments. Limnology and Oceanography, 20: 493–495.

Solorzano, L. 1969. Determination of ammonia in natural waters by the phenolhypochlorite method. Limnology and Oceanography, 14: 799-801.

Thomsen, J., and Melzner, F. 2010. Moderate seawater acidification does not elicit long-term metabolic depression in the blue mussel *Mytilus edulis*. Marine Biology, 157: 2667–2676.

Thomsen, J., Gutowska, M. A., Sapörster, J., Heinemann, A., Trübenbach, K., Fietzke, J., Hiebenthal, C., *et al.* 2010. Calcifying invertebrates succeed in a naturally CO_2-rich coastal habitat but are threatened by high levels of future acidification. Biogeosciences, 7: 3879–3891.

Travers, M.-A., Mirella da Silva, P., Le Goïc, N., Marie, D., Donval, A., Huchette, S., Koken, M., *et al.* 2008. Morphologic, cytometric and functional characterisation of abalone (*Haliotis tuberculata*) haemocytes. Fish & Shellfish Immunology, 24: 400–411.

Travers, M.-A., Basuyaux, O., Le Goic, N., Huchette, S., Nicolas, J.-L., Koken, M., and Paillard, C. 2009. Influence of temperature and spawning effort on *Haliotis*

874 *tuberculata* mortalities caused by *Vibrio harveyi*: An example of emerging vibriosis
875 linked to global warming. Global Change Biology, 15: 1365–1376.
876 Vilchis, L. I., Tegner, M. J., Moore, J. D., Friedman, C. S., Riser, K. L., Robbins, T. T., and
877 Dayton, P. K. 2005. Ocean warming effects on growth, reproduction, and survivorship
878 of southern california abalone. Ecological Applications, 15: 469–480.
879 Waldbusser, G. G., Voigt, E. P., Bergschneider, H., Green, M. A., and Newell, R. I. E. 2011.
880 Biocalcification in the eastern oyster (*Crassostrea virginica*) in relation to long-term
881 trends in Chesapeake Bay pH. Estuaries and Coasts, 34: 221–231.
882 Weiss, I. M., Lüke, F., Eichner, N., Guth, C., and Clausen-Schaumann, H. 2013. On the
883 function of chitin synthase extracellular domains in biomineralization. Journal of
884 Structural Biology, 183: 216–225.
885 Welladsen, H. M., Southgate, P. C., and Heimann, K. 2010. The effects of exposure to near-
886 future levels of ocean acidification on shell characteristics of *Pinctada fucata*
887 (Bivalvia: Pteriidae). Molluscan Research, 30: 125–130.
888 Wessel, N., Martin, S., Badou, A., Dubois, P., Huchette, S., Julia, V., Nunes, F., *et al.* 2018.
889 Effect of CO_2–induced ocean acidification on the early development and shell
890 mineralization of the European abalone *Haliotis tuberculata*. Journal of Experimental
891 Marine Biology and Ecology, 508: 52–63.
892 Winter, B. 2013. Linear models and linear mixed effects models in R with linguistic
893 applications. arXiv:1308.5499.[http://arxiv.org/pdf/1308.5499.pdf]
894 Wittmann, A. C., and Pörtner, H.-O. 2013. Sensitivities of extant animal taxa to ocean
895 acidification. Nature Climate Change, 3: 995–1001.
896 Wolf-Gladrow, D. A., Zeebe, R. E., Klaas, C., Körtzinger, A., and Dickson, A. G. 2007. Total
897 alkalinity: The explicit conservative expression and its application to biogeochemical
898 processes. Marine Chemistry, 106: 287–300.

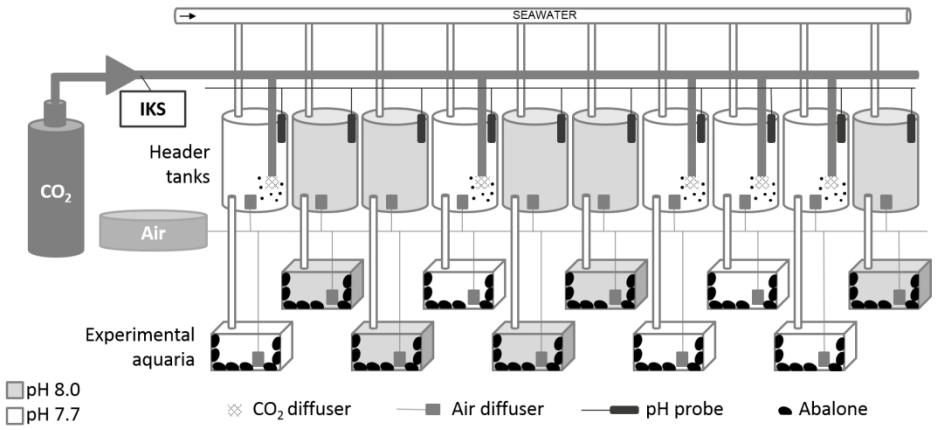

Figure 1. Experimental design. Seawater was continuously pumped into the ten 60-L header tanks. The pH was adjusted in CO_2 enriched header tanks by bubbling CO_2 through electro-valves and controlled by the IKS system (grey tanks for pH 8.0, white tanks for pH 7.7). From the header tanks, the CO_2-enriched water and the control water flowed down to 45L experimental aquaria. Each aquarium contained 26 adult abalone (i.e., there were a total of 130 abalone per pH treatment).

154x85mm (300 x 300 DPI)

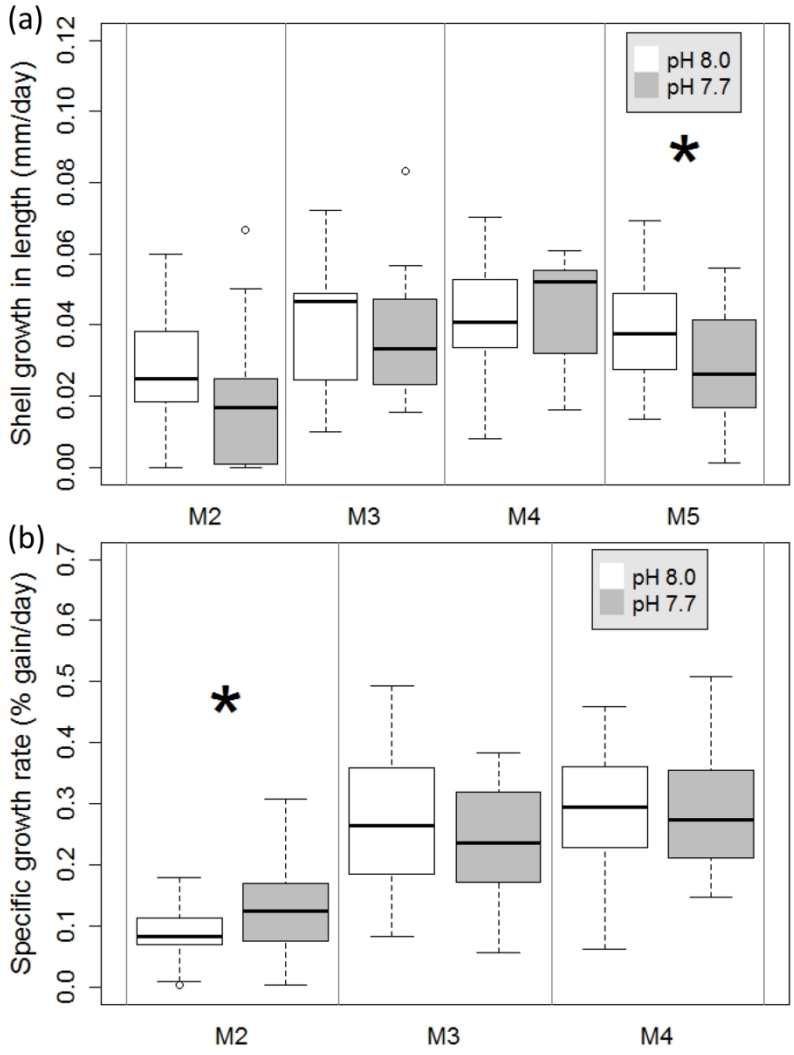

Figure 2. (a) Shell growth in length (n = 13 to 39 per pH treatment) and (b) specific growth rate (n = 13 to 26 per pH treatment) of adult abalone exposed to two pH levels (8.0 and 7.7), after two (M2), three (M3), four (M4) and five (M5) months of exposure. Significant difference is indicated by * ($p < 0.05$, mixed model).

85x122mm (600 x 600 DPI)

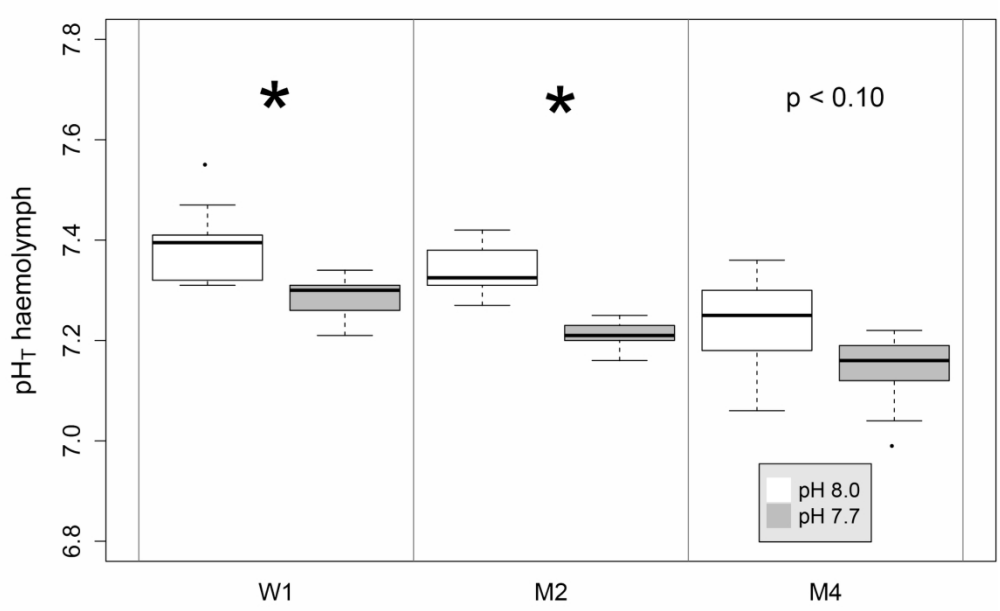

Figure 3. pH_T of adult abalone haemolymph exposed to two pH levels (8.0 and 7.7), after one week (W1), and two (M2) and four (M4) months of exposure (n = 7 to 10 per pH treatment). Significant differences are indicated by * (p < 0.05, mixed model).

85x52mm (600 x 600 DPI)

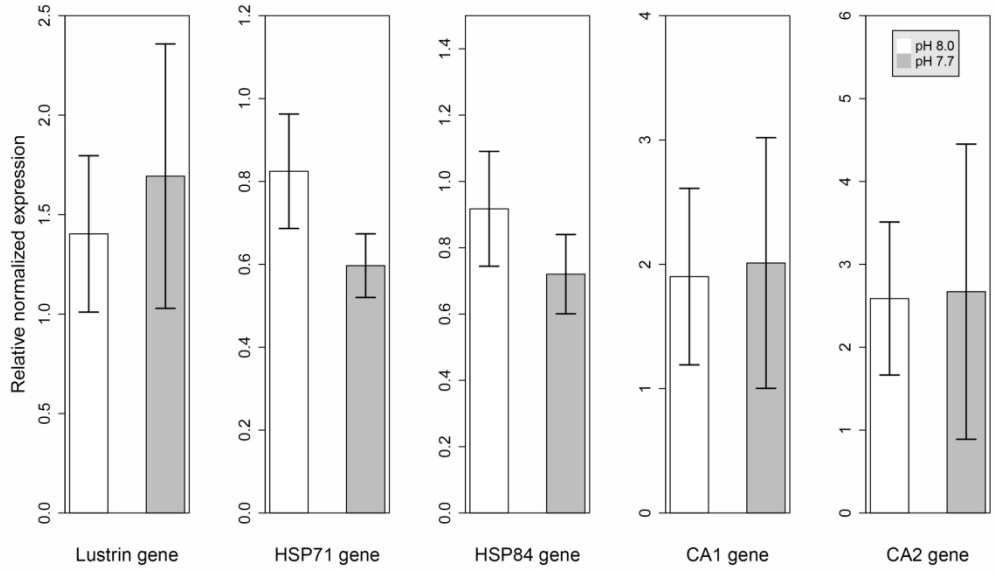

Figure 4. Expression pattern of Lustrin A, HSP71, HSP84, carbonic anhydrase 1 (CA1) and carbonic anhydrase (CA2) genes in the mantle of adult abalone exposed to control (8.0, *n* = 16) and low (7.7, *n* = 14) pH for four months.

85x48mm (600 x 600 DPI)

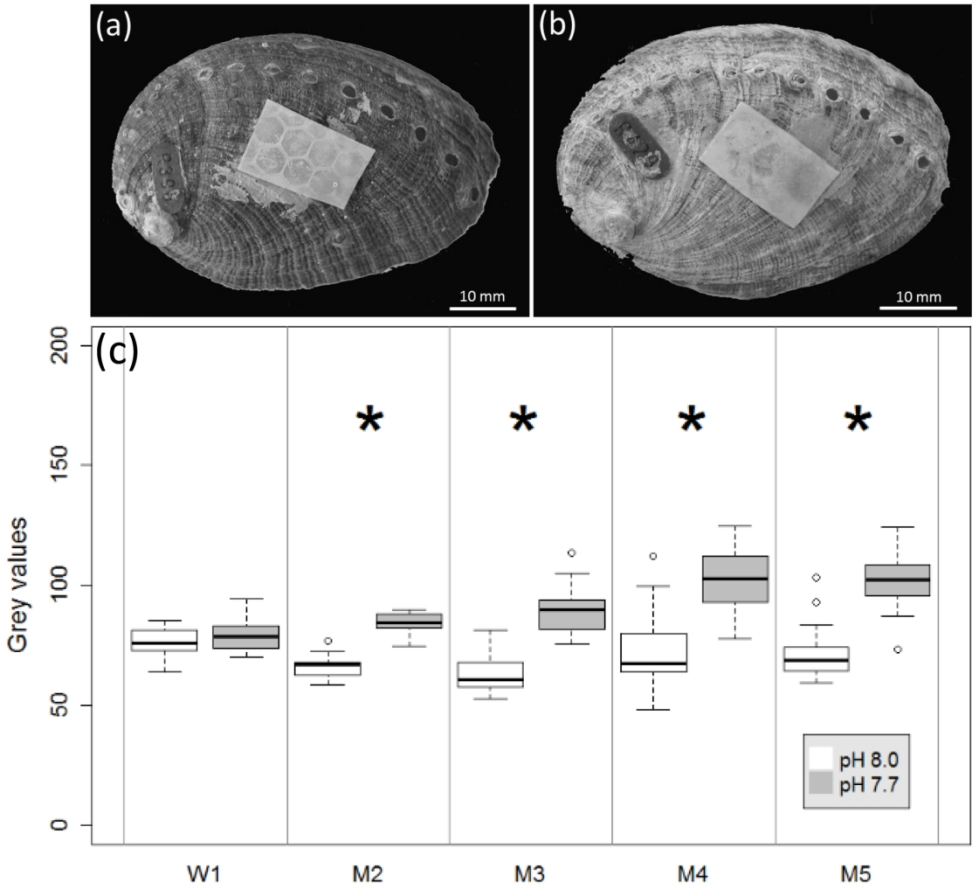

Figure 5. Shell coloration pattern of abalone after five months of exposure to (a) pH 8.0 and (b) pH 7.7 and (c) mean grey values (0: black to 255: white) of abalone shells exposed to two pH values (8.0 and 7.7, n = 10 to 39 per pH treatment) after one week (W1), and two (M2), three (M3), four (M4) and five (M5) months of exposure. Significant differences are indicated by * ($p < 0.05$, mixed model).

84x83mm (600 x 600 DPI)

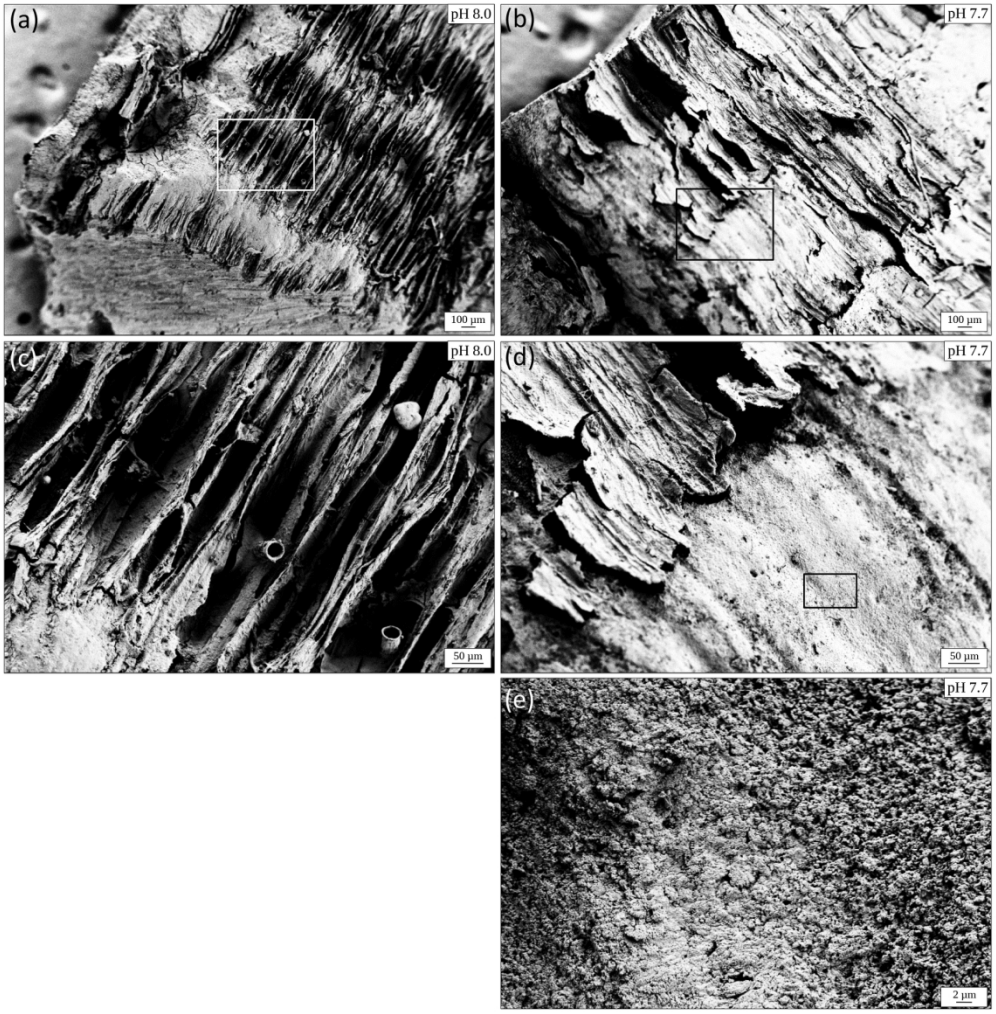

Figure 6. Scanning electron microscopy (SEM) images of the outer shell surface of abalone grown in control conditions (pH 8.0, a, c) and under lower pH (pH 7.7, b, d, e) for four months. (a) & (b) Views of the shell border formed during the experiment. (c) Detail of the periostracum in the control, boxed in (a), showing a homogenous surface with the typical ridge and groove pattern. (d) Detail of the periostracum in the pH 7.7 treatment, showing the delamination of organic layer and revealing the underlying spherulitic layer. (e) Magnification of the corroded area boxed in (d) showing typical biominerals of the spherulitic layer.

170x175mm (300 x 300 DPI)

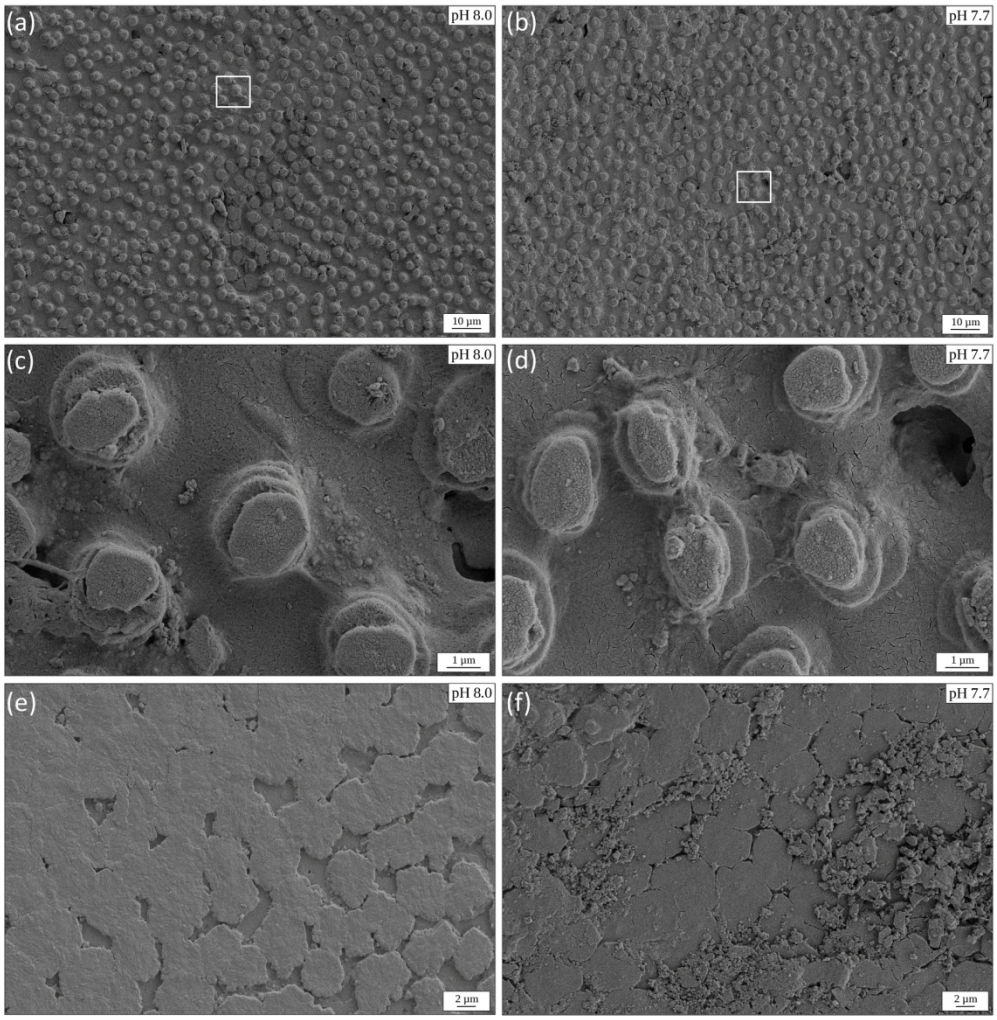

Figure 7. Scanning electron microscopy (SEM) images of the inner nacreous layer in control abalone shell (pH 8.0, a, c, e) and in abalone exposed to pH 7.7 for four months (b, d, f). (a) & (b) Inner nacreous layer showing a homogenous surface with growing aragonite platelets. (c) & (d) Magnification of the nacre growth region, boxed in (a) & (b), respectively. (e) & (f) Detail of the transition region between immature and mature nacre showing dissolution of the aragonite platelets under lower pH (f).

170x176mm (300 x 300 DPI)

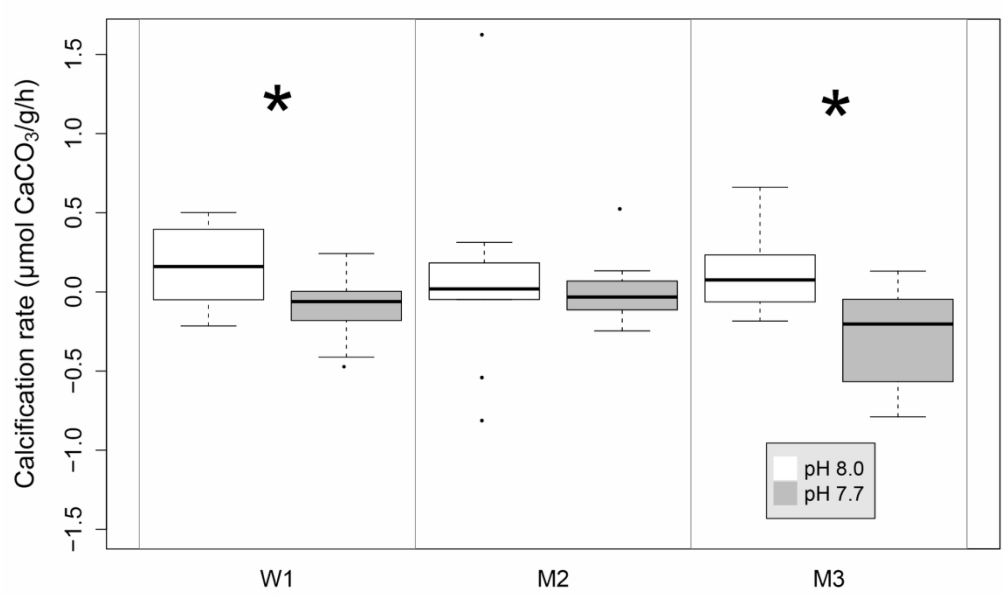

Figure 8. Net calcification rate of adult abalone exposed to two pH values (8.0 and 7.7, n = 9 to 15 per pH treatment) after one week (W1), and two (M2) and three (M3) months of exposure. Significant differences are indicated by * ($p < 0.05$, mixed model).

85x51mm (600 x 600 DPI)

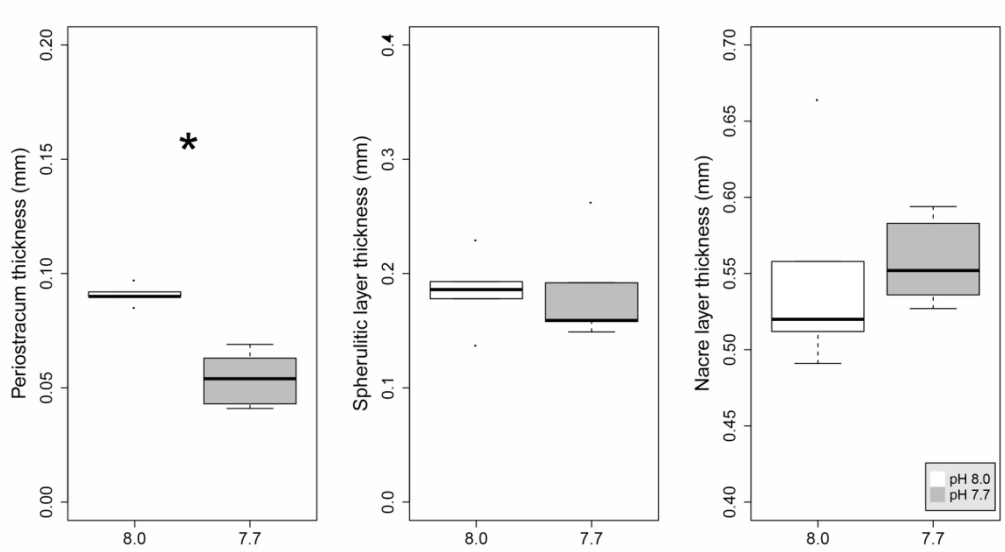

Figure 9. Periostracum, spherulitic and nacre layer thickness of adult abalone after four months of exposure to control (8.0, n = 5) and lowered (7.7, n = 5) pH. Significant difference is indicated by * ($p < 0.05$, mixed model).

85x47mm (600 x 600 DPI)

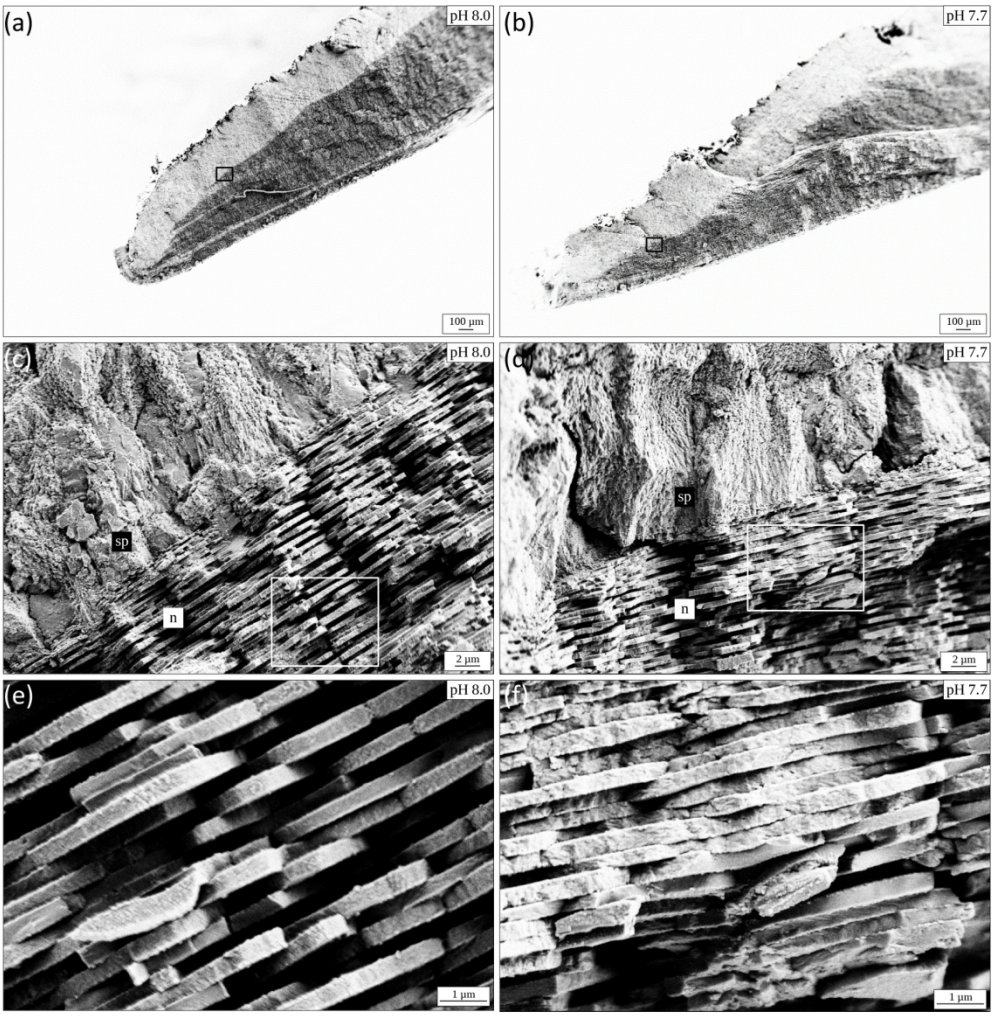

Figure 10. Scanning electron microscopy (SEM) images of shell cross-sections of adult abalone exposed to pH 8.0 (a, c, e) and 7.7 (b, d, f) for four months. (a) & (b). Cross-sections of the newly formed shell. (c) & (d). Detail of the interface between the spherulitic layer (sp) and the nacreous layer (n). (e). Magnification of the nacre layer boxed in (c) showing regular stacks of aragonite platelets. (f). Magnification of the nacre layer boxed in (d) showing pitting corrosion within the aragonite platelets at pH 7.7.

170x173mm (300 x 300 DPI)

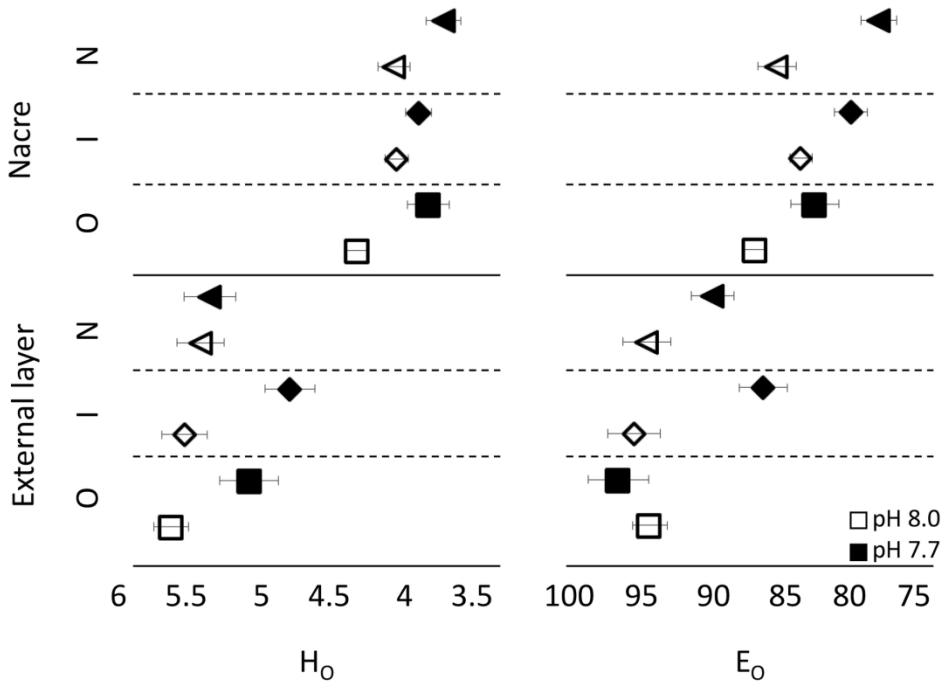

Figure 11. Nanoindentation measures of hardness (H_0) and Young's modulus of elasticity (E_0) in the external layer and in the nacre of abalone shell exposed to two pH values (8.0 and 7.7) for four months (*n* = 4 per pH treatment). O, I and N refer to the shell regions investigated i.e: O: old, I: intermediate and N: new part of the shell. Weibull analysis was used to calculate the 95% confidence intervals of E_0 and H_0 corresponding to 63% of the population with the modified least square regression according to Bütikofer *et al.* (2015).

85x62mm (600 x 600 DPI)